8-8-2008

Axial Ligand Mutant: H229A

Nhung Phuong Nguyen

AXIAL LIGAND MUTANT: H229A

by

NHUNG PHUONG NGUYEN

Under the Direction of Dabney White Dixon

ABSTRACT

Many pathogenic bacteria use their iron acquisition mechanisms to live inside hosts. *Streptococcus pyogenes* is a pathogenic bacterium that uses streptococcal iron acquisition ABC transporter to obtain heme. SiaA (HtsA, *spy1795*), a lipoprotein located on the cell surface, serves as a heme binding protein. To understand the iron-uptake mechanism, histidine 229, one of the two proposed axial ligands in SiaA, was mutated to alanine. SiaA H229A was expressed in *E. coli*, lysed by French Press, and purified by fast protein liquid chromatography (FPLC). SDS-PAGE indicated that pure protein was isolated. Nickel affinity FPLC gave purer H229A when 0.5 M imidazole was added to the binding buffer. Overall, histidine 229 is likely to be an axial ligand in wild type SiaA, as shown by the fact the mutant readily lost heme as evidenced by UV-vis spectra.

INDEX WORDS: *Streptococcus pyogenes,* Heme, SiaA, ABC transport, *E. coli,* axial ligand, histidine, alanine, fast protein liquid chromatography, FPLC, SDS-PAGE, nickel affinity, homology modeling, PBP, bacterial iron acquisition, H229A

AXIAL LIGAND MUTANT: H229A

by

NHUNG PHUONG NGUYEN

An Honors Thesis Submitted in Partial Fulfillment of the

Requirements for Graduation with Undergraduate Research Honors

in the College of Arts and Sciences

Georgia State University

2007

AXIAL LIGAND MUTANT: H229A

by

NHUNG PHUONG NGUYEN

Honors Thesis Director: Dr. Dabney White Dixon
Honors Program Director: Dr. Robert Sattelmeyer

Electronic Version Approved:

Honors Program
College of Arts and Sciences
Georgia State University
December, 2007

AXIAL LIGAND MUTANT: H229A

An Honors Thesis

Presented in Partial Fulfillment of Requirements for Graduation with Undergraduate Research Honors, Georgia State University

2006

by

NHUNG PHUONG NGUYEN

_____

Dr. Dabney Dixon, Honors Thesis Director

_____

Dr. Robert Sattelmeyer, Honors Program Director

December 2007
Date

ACKNOWLEDGEMENTS

I would like to thank Dr. Dabney Dixon for giving me the opportunity to carry out this project. Your input and guidance throughout the research and writing process of this thesis are greatly appreciated. Thank you for making me a strong writer and an independent thinker.

I am grateful to my mentors, friends, and colleagues for lending assistances in introducing new techniques and providing helpful comments and suggestions, especially thank to Brian Sook, Sarah Shealy, Thanh Quach, Brian Basden, and Kyle Chan.

I wish to thank my family, especially to my parents – Ngo and Van Nguyen, for their boundless love, encouragements, motivations, and supports.

Table of Contents

List of Figures

Introduction

Many pathogenic microorganisms use iron acquisition mechanisms to obtain heme. Heme is an essential iron source for many bacteria (Crosa et al., 2004). An understanding of the structure and mechanism of the iron uptake pathways may help in the design agents to control these pathways, possibly resulting in new clinical agents to treat disease.

S. pyogenes uses SiaABC to acquire heme from its host. SiaA, a heme binding protein, is a lipoprotein located on the cell surface. We have proposed that methionine 79 and histidine 229 are the two axial ligands of the heme. In this project, histidine 229 was studied. The native ligand, in wild type SiaA, His229, was mutated by replacing histidine with alanine (H229A). H229A SiaA was expressed, purified, and studied.

Streptococcus pyogenes. *Streptococcus pyogenes* (Group A Streptococcus) is a Gram-positive, non-motile, non-spore-forming coccus (Bates et al., 2005; Bates et al., 2003; Liu & Lei, 2005). It is a facultative anaerobe. *S. pyogenes* has a capsule composed of hyaluronic acid and exhibits beta (clear) hemolysis on blood agar (Cunningham, 2000). It can colonize the respiratory tract, bloodstream, and the skin. It causes severe infections such as pharyngitis (strep throat), toxic shock syndrome, necrotizing fasciitis (flesh eating bacteria), and rheumatic fever.

S. pyogenes exhibits iron-dependent growth (Eichenbaum et al., 1996b). Iron limitation leads to the induction of genes encoding a putative iron transport system, hemolysins, a putative superoxide dismutase, a bacterioferritin homologue, and iron dependent repressors (Bates et al, 2005). *S. pyogenes* produces iron acquisition proteins

(siderophores, hemophores, or specific receptors) to obtain more iron when the concentration is limited (Bates et al, 2003). The bacterium cannot extract iron from transferring or lactoferrin (Eichenbaum et al., 1996a; Eichenbaum et al, 1996b).

Heme or hemoglobin is an essential iron source in vivo (Bates et al, 2003; Bates et al, 2005). Studies in an iron-depleted medium experiment showed that heme in sheep blood aided *S. pyogenes* growth. *S. pyogenes* can also extract heme from myoglobin, heme-albumin, haptoglobin-hemoglobin complexes, and hemopexin:hemoglobin complexes. *S. pyogenes* utilizes surface receptors to bind hemoglobin and other hemoproteins (Bates et al, 2003).

SiaABC. *S. pyogenes* use SiaABC to acquire heme (Figure 1) (Bates et al, 2003; Bates et al, 2005; Liu et al, 2005). SiaABC is the streptococcal iron acquisition ABC transporter (Bates et al, 2003; Bates et al, 2005). Another name for SiaABC is HtsABC, the heme transporter of group A streptococcus (Liu & Lei, 2005). The SiaABC (HtsABC) is made up of three genes in a ten gene cluster: *spy1793, spy1794*, and *spy1795* (Bates et al, 2003; Lei et al., 2003). SiaA (HtsA, *spy1795*) is a lipoprotein located on the cell surface and serves as a heme binding protein. SiaB (HtsB, *spy1794*) is the membrane permease. SiaC (HtsC, *spy1793*) is the ATPase that is uses the energy of ATP for heme import.

SiaA. SiaA binds both hemoglobin and heme (Bates et al, 2003; Lei et al, 2003; Liu et al, 2005). A recombinant form of SiaA (rSiaA) was constructed in which the lipoprotein tail of SiaA at the N-terminus was replaced with a His-tag Xpress epitope (Figure 2)

(Bates et al, 2003). Western blot and SDS-PAGE showed that the recombinant protein bound hemoglobin. Enterokinase (EK) cleavage and hemoglobin-binding assays showed that rSiaA both with and without His-Xpress epitope were able to bind hemoglobin.

In the binding assay experiment, transferrin served as a control and did not bind hemoglobin (Bates et al, 2003). A solid phase binding assay showed that SiaA could form a stable complex with hemoglobin but it could not bind myoglobin or hemoglobin-haptoglobin complexes. However, it can acquire iron from these species, indicating that *S. pyogenes* needs additional proteins to take up heme and transport it to SiaA (Eichenbaum et al, 1996b).

When SiaA was expressed and purified in *E. coli*, the sample shows an intense red color (Bates et al, 2003; Lei et al, 2003; Liu et al, 2005). This was due to the presence of heme in the heme-binding protein. The UV-visible absorption spectrum for SiaA showed peaks at 275, 370, 417, 530, and 560 nm (Lei et al, 2003). The SDS-PAGE indicated that SiaA was about 35 kDa (Bates et al., 2003; Lei et al., 2003; Liu & Lei, 2005). As isolated, recombinant SiaA contained about 0.25 bound heme molecule, whereas reconstituted SiaA contained about 1.0 bound heme molecules (Liu et al, 2005).

ABC Transporters. ATP-binding cassette (ABC) proteins are multi-domain structures that use the energy of ATP hydrolysis to translocate solutes across cellular membranes (Figure 3) (Jones & George, 2004; Jones & George, 2005). ABC transporters are made up of two transmembrane domains (TMDs) and two nucleotide-binding domains (NBDs). The TMDs act as the substrate binding sites, while the NBDs, molecular motors, use ATP energy for conformational change to transport the solutes (Jones et al, 2004). The TMDs

contain multiple hydrophobic segments. They consist of α-helices that form six to eleven membrane spanning regions and form the transmembrane channel. These TMDs are substrate-specific. They connect to an intra-cytoplasmic helix bundle, which interacts with the NBDs.

The NBDs are located in the cytoplasm (Jones et al, 2004). They contain Walker A and B motifs and a highly conserved (C) motif known as the "LSGGQ" motif. The Walker A and B motifs are consensus sequences for nucleotide binding. They are separated by approximately 90 – 120 amino acids. The Walker A motif (G-X-X-G-X-G-K-S/T) is a phosphate binding (P) site consisting of a glycine loop followed by an uncapped α-helix. Its function is to bind the nucleotide through electrostatic interactions with the triphosphate moiety. The Walker B motif contains four hydrophobic residues and an aspartate. The Walker B motif consists of a ß strand within the core of the nucleotide-binding fold. To maintain the geometry of the active site, the Walker B aspartate hydrogen bonds to ligands coordinated to the catalytic Mg^{2+} ion. The C motif is the signature sequence of ABC transporters. It is located after the Walker B sequence.

ABC transporters are found in both prokaryotes and eukaryotes (Jones et al, 2004). They are mostly unidirectional. Eukaryotes use ABC proteins as exporters while prokaryotes use them as importers. In prokaryotes, the Gram-negative ABC protein is a periplasmic binding protein dependent transporter (Higgins, 1992; Higgins & Linton, 2001; Higgins, 2001). The Gram-positive ABC protein is a binding lipoprotein dependent transporter. The importers have four polypeptide subunits (two TMDs and two NBDs) and accessory periplasmic binding proteins (PBPs). In general, each ABC transporter has a PBP fused to each TMD, meaning that there are two substrate transfer

sites at the PBP-TMD interfaces. Eukaryotes exporter do not have PBPs. The exporters are made up of a single polypeptide with the TMD connected to the C-terminal end of each NBD. The ABC importers contain TMDs that range from 8 to 20 transmembrane helices (Locher, 2004). The ABC exporters TMDs have a total of 12 transmembrane helices.

The TMDs and NBDs are organized in the order NH_3^+-TMD-NBD-TMD-NBD-COO^- for a full transporter (Higgins, 1992; Higgins, 2001; Higgins et al, 2001). Sometimes, half-transporters are present in both prokaryotes and eukaryotes. Half-transporters are comprised of one TMD and one NBD. Each TMD is covalently fused to a C-terminal NBD. Otherwise, each TMD is initially fused to an N-terminal NBD then followed by a TMD (Jones et al, 2004). Half-transporters can be homodimers or heterodimers.

The cobalamin ABC transporter: BtuCDF. Btu (B twelve uptake) is an *E. coli* protein assembly that imports vitamin B_{12} (Karpowich et al., 2003). Btu includes the ABC transporter BtuCD, the periplasmic binding protein (PBP) BtuF, and the outer membrane transporter BtuB. In the BtuCD, there are two copies of the membrane-spanning BtuC subunit (Locher & Borths, 2004). There are also two copies of the BtuD subunits which are the nucleotide binding domains. The BtuC and BtuD subunits form a functional heterotetramer ($BtuC_2D_2$). On the interface of the $BtuC_2$ subunits, two pairs of helices in an anti-parallel arrangement form a single translocation pathway. The pathway has a cavity that opens to the periplasmic space and allows the corrin ring of vitamin B_{12} to fit. After binding vitamin $B_{12,}$ the residues in two loops of the cavity are closed to the

cytoplasm. On the cytoplasmic side, the BtuD subunits are aligned such that the nucleotide is bound at the dimer interface. The ATP molecule binds against the P-loop of the opposite subunit. Locher speculates that the membrane spanning BtuC subunits keep the BtuD subunits properly aligned through extensive interdomain interactions (Locher et al, 2004). After hydrolysis, the conformational changes from ATP binding are transmitted through various loops in the conserved NBD region to the BtuC subunit (Borths et al., 2002). Locher has proposed that the amino acid residues of the BtuD subunits involved in the interface with BtuC are clustered around the Q-loop (Locher et al, 2004). The Q-loop acts as a λ-phosphate sensor, which changes the conformation upon nucleotide binding and hydrolysis.

BtuF. BtuF binds vitamin B_{12} and releases it to BtuCD channel (Figure 4) (Borths et al, 2002; Locher et al, 2004). BtuF consists of two globular (α/ß) domains connected by a rigid α-helix, α-6 (Karpowich et al, 2003). Between the two domains, a deep cleft is formed, which is the substrate binding site. Each globular domain has a secondary structure that alternates between α-helixes and parallel β–sheets at the N-terminus. Domain I starts at the N-terminus, while domain II starts at the C-terminus. Both domains are α/ß sandwiches. Domain I consists of five-stranded parallel ß-sheet with α-helix connected to each strand. Its α-5 helix lies against the interdomain α-6 helix to form a partial helical bundle, which contacts the B_{12} at its dimethylbenzimidazole (DMB) and propionamide groups. Domain II consists of a four stranded parallel ß-sheet with connecting α-helix. Instead of α-5 helix, the C-terminal helix (α-11) packs against the interdomain α-6 helix.

The B_{12} binding site of BtuF is acidic while the protein itself is basic (Karpowich et al, 2003). About 60% of the B_{12} is inside the binding cleft, held in by 11 residues that make direct contacts with B_{12} in both of the crystal structure monomers. Domain I contacts B_{12} 50 times with six residues while domain II uses 5 residues to contact B_{12} 39 times.

Iron acquisition in bacteria. Many pathogenic bacteria use their iron acquisition mechanisms to live inside hosts. Iron acquisition is necessary because free iron is an important nutrient factor for bacterial infection (Skaar & Schneewind, 2004). Although humans have an abundant amount of iron, essentially all of it is bound, largely by proteins. An iron limited environment is a hostile environment for the growth of bacteria unless they have mechanisms to access these bound iron atoms. In humans, hemoproteins (largely hemoglobin and myoglobin) contain the majority of iron atoms (Mazmanian et al., 2003). Erythrocytes carry 60 – 75% of the body's iron content in hemoglobin. When erythrocytes lyse, hemoglobin is degraded and heme is released. Free heme is not tolerated by cells. Hemopexin binds the free heme and transports it back to the liver.

***Staphylococcus aureus* Isd System.** *S. aureus* has an iron regulated surface determinant (Isd) system which is capable of binding and transporting heme (Skaar et al, 2004). There are two ways that *S. aureus* obtains both free heme and hemoproteins and uses them as iron sources. One of these is through siderophore-dependent mechanisms. These use an iron chelator that has a high affinity for iron to remove and transport iron

atoms from host proteins into the bacterial cell. Another way is through Isd gene clusters, which are only transcribed when concentrations of iron atoms are low.

The Isd system of *S. aureus* consists of IsdA, IsdB, IsdC, IsdD, IsdE, IsdF, SrtB, IsdG, IsdH, and IsdI (Figure 5) (Skaar et al, 2004; Skaar et al., 2004). These transcriptional units are made up of cell-wall anchored surface proteins (IsdABCH), a membrane transporter (IsdDEF), a sortase (SrtB), and two cytoplasmic proteins (IsdGI). The IsdABCH, IsdDEF, and IsdGI are involved in binding heme, while sortase acts as an enzyme to covalently attach specific proteins, to the cell wall.

Sortase-mediated cell wall anchoring pathway. Sortases, membrane anchored transpeptidases, are enzymes that catalyze amide linkage formation between the cell wall peptidoglycan and the C-terminus of a protein (Jonsson et al., 2003; Skaar et al, 2004). These enzymes are also used to cleave LPXTG motifs of the protein. The LPXTG motif is made up of five amino acids: leucine, proline, X, threonine, and glycine, where X is any amino acid. The LPXTG motif, a hydrophobic region, and a tail of charged residues, all located near the carboxyl terminal, are the three factors that are necessary for the covalent adhesion between proteins and cell wall peptidoglycan (Paterson & Mitchell, 2004). They act as the cell wall sorting signal.

There are two types of sortases, sortase A and sortase B. Sortase A anchors the LPXTG motif (IsdA, IsdB, and IsdH) of the Isd system to the bacteria cell wall (Jonsson et al, 2003). Sortase A recognizes the LPXTG motif by detecting acidic residues and the hydrophobic region of these three proteins (Skaar et al, 2004). Most of the time, sortase A is active. When sortase A is inactivated, a covalent linkage between bacteria cell wall

and the protein cannot be established. Sortase A substrates are anchored to the pentaglycine crossbridge of the staphylococcal cell wall; the inability to covalently anchor the proteins to the cell wall affects bacterial virulence. Sortase B (srtB) anchors isdCDEFsrtBisdG proteins, which are involved in binding heme, to the cell wall of the bacteria.

The Isd proteins in sortase A and sortase B are under the regulation of the iron-dependent repressor Fur, a ferric-uptake regulator protein (Skaar et al, 2004; Jonsson et al, 2003). Fur is a repressor gene that controls the production of Isd proteins (Maresso & Schneewind, 2006). Fur functions as a regulator that senses and responds to the need to acquire iron from the environment. When bacteria sense the exhaustion of iron, Fur activates the production of Isd proteins. Sortase B, IsdA, IsdB, IsdC, and IsdH can then be assembled to ensure successful nutrient acquisition.

Inactivation of sortases reveals that the Isd system has a role in uptake of heme iron atoms into the bacteria (Skaar et al, 2004). With the inactivation of sortase A, the level of heme iron in *S. aureus* is decreased due to the reduction of heme being transported into the cell. As the result, *S. aureus* does not have the ability to bind to hemoglobin as before and its virulence is diminished. Sortase B does not reduce bacteria virulence greatly when it is inactivated. However, it reduces the persistent infection of *S. aureus* in tissues. This is thought to be due to an inability to acquire heme iron atoms from the host through the loss of IsdC anchoring.

Perisplasmic binding protein. Most PBPs contain two globular domains that are connected by a hinge region (Eakanunkul et al., 2005). The pocket between the two

domains forms the binding site. The PBP consists of three groups. Group I has three interdomain connections, group II has two interdomain connections, and group III has one interdomain connection (α-helical). The proteins BtuF and FhuD are part of group III PBPs and sequence homology suggests that ShuT is also a Group III PBP.

ShuT. ShuT, a PBP, binds heme in *Shigella dysenteriae* (Eakanunkul et al, 2005). It transports heme to the proteins ShuUV, which are a cytoplasmic permease and an ATPase. The sequence of ShuT is similar to the sequences of BtuF and FhuD.

ShuT is a monomeric protein (Eakanunkul et al, 2005). SDS-PAGE and size exclusion chromatography show that ShuT has a molecular weight of approximately 28.5 kDa. ShuT binds one *b*-type heme per monomer. Tyr94 is the only axial ligand. Tyr228 helps to stabilize the interaction between the ligand and ShuT; it does not directly interact with heme iron.

FhuD. FhuD, a PBP, binds hydroxamate-type siderophores in *E. coli* (Clarke et al., 2002b; Clarke et al., 2002a; Krewulak et al., 2005; Carter et al., 2006). It obtains siderophores from FhuA, an outer membrane receptor, and transports them to FhuBC, the inner membrane ATP-binding cassette transporter. FhuD has a molecular mass of 32 kDa. It has two distinct domains that are connected by a long α-helical backbone. The N-terminal domain consists of five β-sheets and four α-helices while the C-terminal domain has two β-sheets with three α-helices. The shallow pocket between the two domains makes up the siderophore binding site. The pocket is hydrophobic and has

aromatic residues. The movement of amino acid side chains in the binding cleft allows a variety of hydroxamate-type siderophores to bind.

Siderophores bind to FhuD through both hydrophobic and hydrophilic interactions (Clarke et al, 2002b; Clarke et al, 2002a; Carter et al, 2006). When the siderophore binds, its methylene carbon atoms form hydrophobic interactions with aromatic FhuD residues. There are three hydrogen bonds formed between albomycin and FhuD. Two of the hydrogen bonds form between the hydroxamate and the FhuD residue Arg84 while the other forms between the hydroxamate and Tyr106. Similar to the albomycin binding, the interactions between gallichrome and FhuD also show hydrogen bonding, except that there is an intermediate water molecule.

MntC. In *C. synechocytis,* MntC is the periplasmic binding protein for the manganese (Mn^{2+}) ABC transport system (Rukhman et al., 2005). MntC has two globular domains connected by an α-helix. His89, His154, Glu220, and Asp295 are proposed to be the ligands to the manganese. The metal ion-binding site is asymmetric in that the two negatively-charged residues are located closer to the manganese ion than the two histidine residues.

The crystal structure of MntC shows three monomers (A, B, and C) in the unit cell (Rukhman et al, 2005). Each monomer has four domains: the N-terminal upper globular domain, the α-helical backbone, the lower globular domain, and the C-terminal domain.

MntC has a disulfide bond between Cys219 and Cys268 close to the surface (Rukhman et al, 2005). Cys219 is located before Glu220, which binds Mn^{2+}. The loop

that contains Cys268 is in contact with the loop that contains Asp295, which also binds Mn^{2+}. Reduction of the disulfide bond lowers the affinity of MntC toward Mn^{2+}.

Monomer C is more disordered that either A or B (Rukhman et al, 2005). Most of the disordered region is localized in the lower domain. The disulfide bond in this monomer has weaker electron density, which may indicate that the cysteine side chains adopt a number of conformations. The poor electron density on Glu220 shows that this residue is flexible. The electron density at the Mn^{2+} of monomer C is weaker than the density at the Mn^{2+} of monomers A and B, indicating there is a lower metal ion occupancy in this monomer. The Mn^{2+} binding site is also 0.5 Å further from Glu220 and closer to His89. Rukhman et al. propose that the disulfide bond in monomer C is heterogeneous, with partial reduction leading to movements in the lower domain (Rukhman et al, 2005).

HasA. HasA is an extracellular heme binding protein. It is secreted by bacteria; its function is to bind heme and transport it to an outer membrane receptor. Most studies have been performed on the protein from *Serratia marcescens* (Deniau et al., 2003; Deniau et al., 2001). The crystal structure shows that the holoprotein is made up of four α-helices and six β-sheets (Arnoux et al., 1999). The four α-helices are on the same side of the protein. The two loops at the interface between the α-helices and the β-strands hold the heme. The heme propionates point toward the solvent. With hydrophobic binding pocket residues, heme binding maintains its stability through the help of polar interactions. These include three hydrogen bonds that interact with propionate groups,

two axial bonds, and a network of hydrogen bonds between the core of the protein and residues of the binding pocket.

The axial ligands are histidine (H32) and tyrosine (Y75). Through hydrogen bonding, asparagine (N41) and histidine (H83) residues are linked to the axial ligands. Asparagine, glycine, and tyrosine (N34, G35, and Y137) residues are linked to heme propionate groups.

The tyrosine (Y75) is bound to the heme iron with the bond length of 2.0 Å while histidine (H32) is bound to the heme with the bond length of 2.32 Å. Studies of mutation of Y75 (Y75A) suggests that H83 can replace Y75 in binding heme (Arnoux et al, 1999). Although H83 does not directly bind the iron, evidence from thermodynamics experiments show that H83 is the main factor in affecting the heme binding. When alanine (H83A) or glutamine (H83Q) replaces histidine, the affinity of the heme binding is reduced by 260 and 150 times, respectively. Comparing to the mutation of histidine axial ligand (H32A), the mutation of H83 induces a higher loss of affinity. The interaction of H83 with Y75 indicates that the hydrogen bonding enhances the nucleophilic of Y75. It helps holding the tyrosine ring in the correct orientation so that Y75 can bind to iron.

Campylobacter jejuni. *Campylobacter jejuni* is a rod-shaped, curved pathogenic bacterium that causes food borne infection, especially diarrhea (Muller et al., 2006). *C. jejuni* is a gram negative bacterium and is commonly found in animal feces. *C. jejuni* needs iron (Fe) to survive.

C. jejuni uses the enterobactin siderophore to take up iron (Muller et al, 2006). Enterobactin is an iron chelator and consists of triscatechol (metal binding units) that are linked via amides to a triserine ring (the backbone). Enterobactin chelates iron through triscatechol ligands, forming a Δ configuration.

CeuE is a ferric enterobactin binding protein of *C. jejuni* (Muller et al, 2006). CeuE is made up of α-helices and β-strands; the majority of the protein consists of α-helices. Two α-helices span the protein, while six β-strands are located at one end of the protein and seven are located at the other.

Enterobactin binds iron, forming a ferric-enterobactin complex (FeEnt) (Raymond & Dertz, 2004) (Raymond et al., 2003; Raymond et al, 2004). A cell surface receptor protein recognizes the FeEnt and transports it into the periplasm. Subsequently, the periplasmic binding protein, CeuE, binds the FeEnt and transfers it to a membrane-bound protein that transports it to the cytoplasm.

H_6-mecam is one of the synthetic tris-catecholamide ligands that mimic enterobactin (Muller et al, 2006). CeuE recognizes H_6-mecam through a combination of the α-helices, β-strands, and loops. There is no direct binding between iron and the protein. The residues closest to the H_6-mecam are Arg249, Tyr288, Arg205, Arg118, and Lys121.

Materials and Methods:

Homologous structure: 3D-JIGSAW. The sequence of wild type SiaA was submitted to the 3D-JIGSAW website (http://www.bmm.icnet.uk/servers/3djigsaw/). The homologous structures for BtuF (1N4D) were selected. The graphical coordinates of the homology models (starting with the line ATOM 1) were saved as a txt file. The file was renamed as a pdb file and opened with Rasmol 2.7.2.2.2.1 (originally developed by Roger Sayle).

Homologous structure: LOOPP. The sequence of wild type SiaA was submitted to the LOOPP website (http://cbsuapps.tc.cornell.edu/loopp.aspx). The homologous structures for BtuF (1N4A), CeuE (2CHU), and FhuD (1K7S) were selected. The graphical coordinates of the homology models (starting with the line ATOM 1) were saved as pdb files and opened with Rasmol.

General. UV-vis spectra were taken on a 50-Bio (Varian, Palo Alto, CA) UV-visible spectrophotometer. Water (18.2 MΩ) was from a NANOpure Diamond™ water purifier (Barnstead International, Dubuque, IA). The H229A mutant was a gift of Dr. Zehava Eichenbaum (2aH XUB LB-AMP), stored in a cryovial at -80 °C.

Preparation of Luria-Bertani media. Luria-Bertani (LB) media (2 L) was prepared with 20 g Bacto™ Tryptone (Becton Dickinson, Sparks, MD), 20 g NaCl, and 10 g Bacto® Yeast Extract (Becton Dickinson) in 1940 mL water. The solution was adjusted

to pH 7.0. The broth was autoclaved on a liquid cycle for 45 min and allowed to cool. Ampicillin (amp) stock solution (100 mg/mL) was made by dissolving 1000 mg ampicillin sodium salt (Fisher, Fairlawn, NJ) in 10 mL of sterile water. Ampicillin stock solution (2 mL) was added to the 2 L sterile broth. The resultant solution (2 L LB + 2 mL amp broth) was stored at 4 °C.

A second complete protocol was performed as above except that 3 L of broth was made with 30 g Bacto™ Tryptone (Becton Dickinson, Sparks, MD), 30 g NaCl, and 15 g Bacto® Yeast Extract (Becton Dickinson) in 2910 mL water with 3 mL amp broth.

Inoculation of LB media and the growth of H229A. From the 2 L of LB + 2 mL amp broth, 100 mL were transferred to each of the two 125 mL Erlenmeyer flasks. A loop of mutant H229A was transferred into each flask. The broth was stirred with the same inoculating loop. The cryovial containing H229A was immediately put back into the -80 °C freezer. Both flasks were covered with slightly loosened aluminum foil that allowed air to circulate and were incubated for 16 h at 37 °C with shaking at 200 rpm. The broth had an OD_{660} of approximately 1. The remaining LB media was divided into two 3000 mL Erlenmeyer flasks (~900 mL each). To each flask, 100 mL inoculated broth with H229A was added. Two 3000 mL flasks were again placed in the shaker for 3 h at 37 °C with 200 rpm.

A 2.0% arabinose stock solution was prepared by diluting 4 g of L-arabinose (Acros Organics, Morris Plains, NJ) in 200 mL of water. The solution was vortexed to dissolve the solid and filtered through a 0.20 µm MF75 Nalgene filter unit (Nalgene Labware, Rochester, NY).

After 3 h of shaking, arabinose stock solution (0.05 mL) was added to each flask. The flasks continued to inoculate at 37 °C with shaking at 200 rpm for 4 h.

Similar to the first run, a second complete protocol was performed as above except that 100 mL were transferred to each of the three 125 mL Erlenmeyer flasks. After 16 h of incubation, the growth media was cloudy and had an OD_{660} of approximately 2.8 (using LB broth as a baseline). The remaining LB media was divided into three 2800 mL Erlenmeyer flasks (~900 mL each). To each flask, 125 mL inoculated broth with H229A was added. Three 2800 mL flasks were again placed in the shaker for 3 h at 37 °C with 200 rpm. After 3 h of shaking, the growth media had an OD_{660} of approximately 2.5. The arabinose stock solution (5.0 mL) was added to each flask. The flasks continued to inoculate at 37 °C with shaking at 200 rpm for 4 h. The growth media had an OD_{660} of approximately 5.

Centrifugation. The inoculated sample was transferred to eight sterile plastic centrifuge bottles and centrifuged at 8000 x g for 10 min at 4 °C (Eppendorf Centrifuge 5804 R). The supernatant was discarded. The collecting pellets were placed in cryogenic vials and stored in the freezer at
-20 °C.

French press procedure. Extraction buffer was prepared by dissolving 2.42 g of 20 mM Tris (Fisher Chemicals, Fair Lawn, NJ), 5.84 g of 100 mM NaCl (Aldrich Chemical Company, Milwaukee, WI), and 1 mL of neat 0.1% Triton (MP Biomedicals) in 1 L water to give a buffer solution of 50 mM Tris. The extraction buffer was adjusted to pH

8.0 using HCl. To each of three falcon tubes, two Complete Mini EDTA-free protease inhibitor tablets (Roche Diagnostics, Indianapolis, IN) were dissolved in 30 mL of extraction buffer. Each tube was vortexed until the tablet was dissolved. The solutions were allowed to stand until the bubbles had dissipated. Approximately 9 g of cell pellets were diluted 1:10 by mixing with extraction buffer at 4 °C. This solution was divided equally onto the three falcon tubes and mixed with extraction buffer by vortexing. The falcon tubes were placed on ice. Using a SIM-AMINCO Spectronic Instruments French R Pressure Cell Press, each faction was French pressed at a setting of 1200-1280 on the high ratio unit. Each drop was collected in a falcon tube on ice. Each sample was French pressed twice. The samples were centrifuged at 12000 *x* g for 10 min. The 90 mL of supernatants were collected and the pellets were discarded. Supernatants were concentrated to 35 mL using 15 mL cellulose 5,000 MWCO tube in an Amicon Ultra centrifugal filter device (Millipore, Billerica, MA).

A second complete protocol was carried out as above except that 100 mL of glycerol (Fisher Scientific, Fair Lawn, NJ) was added into the extraction buffer to make 50 mM Tris plus 10% glycerol. To each of two falcon tubes, two Complete Mini EDTA-free protease inhibitor tablets (Roche Diagnostics, Indianapolis, IN) were dissolved in 45 mL of extraction buffer. Each tube was vortexed until the tablets were dissolved. The solutions were allowed to stand until the bubbles had dissipated. Approximately 5 mL of cell pellets were added into each of the falcon tube and mixed by vortexing. The falcon tubes then placed on ice. Using a SIM-AMINCO Spectronic Instruments French R Pressure Cell Press, each faction was French pressed at a setting of 1200-1280 on the high ratio unit. The output was collected in two falcon tubes on ice. These samples were

treated again with the French press and the output collected as second time. The samples were centrifuged at 20,000 *x* g for 25 min. The supernatants (~100 mL) were collected and syringe filtered using a sterile Millex-HV Syringe Driven filter unit with 0.45 μm PVDF filter (Millipore, Bedford, MA) into three falcon tubes. One of these tubes was used for nickel affinity purification (below) and the other two were stored at -80 ^{o}C. The pellets were discarded.

Nickel affinity fast protein liquid chromatography (FPLC) preparation. Extraction buffer (1 L) was prepared as described above. Binding buffer (buffer A) was prepared as follows. K_2HPO_4 (87.09 g) was dissolved in a 500 mL volumetric flask of water. KH_2PO_4 (68.05 g) was dissolved in a second 500 mL volumetric flask of water. The first solution (80.2 mL) and the second solution (19.8 mL) were placed in a 2 L Pyrex bottle. To this was added 29.22 g of NaCl and water added to make a 2 L solution. The pH was adjusted to 7.4; and the solution was filtered by using a 0.45 μM pore size in a Nalgene vacuum filter unit (Nalgene, Rochester, NY). The final solution was 50 mM potassium phosphate with 250 mM NaCl at pH 7.4.

Buffer B (elution buffer) was prepared by diluting 68.08 g of 0.5 M imidazole in 1 L of Buffer A. The final solution (2 L) was vacuum filtered before use. Stripping buffer (1 L) was prepared by adding 18.61 g of 0.05 M 2 Na-EDTA to 1 L of Buffer A. The pH was made to 7.4, the solution was vacuum filtered before use. A 100 mL nickel charging solution was prepared by adding 2.38 g of 0.1 M $NiCl_2$ (Mallinckrodt Chemical Works, St. Louis, MO) to a 100 mL volumetric flask and diluting with water to 100 mL. The solution was vacuum filtered before use.

A HiTrap® Chelating HP nickel column (GE Healthcare Bio-sciences) was washed with 5-10 column volumes (1 CV = 5 mL) of water prior to charging to remove any contaminants present. The column was washed with 5-10 CV of stripping buffer, then at least 5-10 CV of binding buffer, and then 5-10 CV of water at 4.0 mL per min with a pressure under 0.3 MPa. The column was charged with 4 CV of nickel charging solution at 0.5 mL per min. The column was then washed with 5 CV of water and 5 CV of binding buffer at 4.0 mL per min. Pump A, pump B, and the 5 mL column were washed with water. The column was equilibrated with 5 CV binding buffer at 4.0 mL per min. The 50 mL super loop was washed with water. The H229A sample was injected into the super loop. Line A was placed into the binding buffer and line B was placed into the elution buffer. The flow rate of the injection gradient elution was set at 0.2 mL per min with the column pressure limit of 0.3 MPa. The fractions were collected in disposable glass culture tubes. Fractions 1-9 and 15-30 were kept and the rest discarded. After the run, the pumps were washed with water and then with 20% aqueous ethanol for storage.

A second complete protocol was performed as above except that Buffer A and Buffer B had 10% glycerol in each (a gift of Brian Sook, Georgia State University). For this run, fractions 16-33 were kept and the rest discarded.

The sample from collected fractions was taken for UV-vis spectrum through using cord cell. Buffer A was used for the baseline.

Gel electrophoresis. A 1.5 M Tris pH 8.8 buffer was made by dissolving 36.34 g Tris (FisherBiotech, Fair Lawn, NJ) in water to make a 200 mL stock solution. The pH was

adjusted to 8.8 using HCl. A 1.0 M Tris pH 6.8 buffer was prepared by diluting 11.11 g Tris in water to make a 100 mL stock solution. The pH was adjusted to 6.8 using HCl. The 10% sodium dodecyl sulfate (SDS) was made by mixing 1 g SDS (Fisher, Fair Lawn, NJ) in 10 mL water. The 10% APS, ammonium persulfate, was prepared by suspending 1 g ampicillin sodium salt (FisherBiotech, Fair Lawn, NJ) in 10 mL of water. Two plates of 1.0 mm gels were made by preparing 15% resolving layer (bottom layer) and 5% stacking layer (top layer). Resolving layer was prepared by dissolving 2.3 mL water, 5.0 mL of 30% bisacrylamide (FisherBiotech, Fair Lawn, NJ), 2.5 mL of 1.5 M Tris pH 8.8, 100 µL of 10% SDS, and100 µL of 10% APS. Immediately before putting the gels solution into the gels maker, 4 µL TEMED (N,N,N',N'-tetra-methyl-ethylenediamine, Bio-Rad Laboratories, Hercules, GA) was added onto the solution and inverted five times to mix. The gel solution was filled up to 2/3 of the plate. A 1 mL of 2-propanol (Fischer Chemicals, Fair Lawn, NJ) was added onto the gels maker. While waiting for the resolving layer to solidify, a stacking layer was prepared by dissolving 6.8 mL water, 1.7 mL of 30% bisacrylamide, 1.25 mL of 1.0 M Tris pH 6.8, 100 µL of 10% SDS, and 100 µL of 10% APS. When the resolving layer had solidified, water was used to remove the 2-propanol. Filter paper was used to remove the water. TEMED (10 µL) was added to the stacking solution and inverted five times to mix. The solution was then added onto the top of the resolving layer. The 1.0 mm comb was added to the gel maker to make lanes. After the gels had solidified, both gels were washed with water under light pressure, wrapped with moisture paper towels, and kept in the refrigerator at 4 °C.

SDS-PAGE of nickel affinity FPLC fractions. The gels were loaded into a Mini PROTEAN® 3 Cell (Bio-Rad). A 500 mL running buffer at pH 8.3 was prepared by diluting 50 mL of 10 X Tris-glycine-SDS buffer (Fisher cat. BP1341-1) with 450 mL water. The running buffer was poured into the Mini PROTEAN® 3 Cell. Mixed Laemmli sample buffer was made by adding 50 μL 2-mercaptoethanol (Bio-Rad) with 450 μL of Laemmli sample buffer (Bio-Rad). A 5 μL sample was taken from each of the affinity FPLC fractions 4, 6, 16, 17, 18, 21, 23, 25, 27, and 28. Each of these was mixed with 10 μL of mixed Laemmli sample buffer. Samples were centrifuged for 15 sec on a VWR mini-centrifuge C-1200 and heated for 5 min at 103°C. Five μL of Precision Plus Protein® molecular weight marker standard (Bio-Rad) were added to lane one. Heated samples were loaded into the remaining gel lanes. The gel was run at 60 – 80 V until the blue Laemmli sample buffer band was 1 cm below the lanes, at which point the voltage was increased to 100 – 120 V until the dye reached the bottom of the gel.

Destaining solution was made by combing 5 parts methanol (Fisher) to 1 part glacial acetic acid (EMD Chemicals, Gibbstown, NJ) and 4 parts water. A Coomassie® Blue staining solution was prepared by dissolving 0.25 g of Coomassie® Brilliant Blue R-250 (Bio-Rad, Hercules, CA) into 100 mL of destaining solution. The gels were removed and stained in the staining solution for 30 min and destained for 2 h on a rotary shaker. The gels were washed with deionized water three times for two min each. The water was emptied and Gel-Dry^{TM} Drying solution (Invitrogen, Carlsbad, CA) was added. The gel was equilibrated by shaking the gel for 20 min in the StainEase^{R} Gel Staining Tray. The gel was removed and placed between two celloplane sheets.

A second complete protocol was performed as above except that mixed Laemmli sample buffer was made by adding 25 µL 2-mercaptoethanol (Bio-Rad) with 475 µL of Laemmli sample buffer (Bio-Rad)**.** A 5 µL sample was taken from each of the affinity FPLC fractions 18, 19, 22, 23, 24, 25, 26, 27, 28, 29, 30, 31, 32, 33, 34, and 35.

The gels were removed and stained in the staining solution for 45 min and destained overnight (approximately 12 h) on a rotary shaker.

Exchanging imidazole buffer into 10 mM Tris pH 8 to remove salt for anion exchange FPLC. A solution of 10 mM Tris pH 8.0 was prepared by dissolving 10 mL of 1 M Tris Buffer pH 8 stock solution (FisherBiotech, Fair Lawn, NJ) in 990 mL of water and the pH adjusted to 8.0. The solution was filtered using a 0.45 µM pore size surfactant free cellulose acetate membrane in a Nalgene vacuum filter unit (Nalgene, Rochester, NY). Fractions 25 through 31 from the first run of the nickel affinity FPLC were combined and placed into three Amicon Ultra 15 filter units with a 5,000 MWCO Ultracel membrane (Millipore, Billerica, MA). The tubes were centrifuged at 5000 *x* g for 15 min at 4°C. Approximately 5 ml of 10 mM Tris was added to the remaining protein solution in each tube and the tubes were centrifuged in the same manner again. This process was repeated 4 times and yielded a total of 4.5 mL of a solution of protein in 10 mM Tris pH 8.

Anion exchange FPLC. Starting buffer was prepared by adding 10 mL 1 M Tris (Fisher, Fair Lawn, NJ) to 990 mL of water. The solution was filtered as described above and adjusted to pH 8.0 by adding HCl. Elution buffer was made by mixing 500 mL of

start buffer with 500 mL of 1 M NaCl (which was prepared by diluting 29.22 g of NaCl in 500 mL of water). The solution was filter and adjusted to pH 8.0 as described above.

The FPLC was fitted with a HiTrap^{TM} Q HP 5 mL (GE Healthcare Bio-sciences) column and washed with water. Pumps A and B were also washed with water. The column was washed with ten CV of anion exchange start buffer (10 mM Tris-HCl pH 8.0), five CV of anion exchange elution buffer (anion exchange start buffer and 1.0 M NaCl), and then equilibrated with seven CV of anion exchange start buffer. The 4.5 mL protein solution was loaded into the superloop and injected into the column. Elution of the protein was performed by running five CV of anion exchange start buffer through the column followed with a 10 CV linear gradient. The gradient began with 100% anion exchange start buffer and ended with 100% anion exchange elution buffer. Fractions 6 to 11 were collected.

Exchanging imidazole buffer to water for mass spectrometry. From second run, fraction 32 (25 μL) was placed in a Microcon Utracel YM-3 filter unit with 3,000 MWCO (Millipore, Bedford, MA). The sample was centrifuged at 3000 *x* g for 45 min at 4°C. The sample was centrifuged for additional 20 min until the sample was reduced to 10 μL. Water (20 μL) was added onto the sample which was centrifuged for 45 min. The process was repeated ten times. ESI and MALDI mass spectra were taken; the sample still contained too much salt.

A second protocol was performed as above except that the sample (20 μL) was centrifuged at 1400 *x* g for 45 min. This process repeated twice until the sample dropped to 7 μL. Water (30 μL) was added and centrifuged two times for 60 min each. Another

20 µL water was added and centrifuged 60 min. This step was repeated a second time. ESI and MALDI mass spectra were taken. The former was not successful; data for the latter are shown.

SiaA thermal stability: Initial practice on myoglobin. Phosphate buffer (50 mL) was prepared by mixing 2.5 mL of KH_2PO_4 with 3.97 mL of K_2HPO_4 in a falcon tube, and making the solution up to 50 mL. A sample of myoglobin (100.0 µL solution of myoglobin in 10 mM Tris pH 8.0 was diluted in 1.00 mL of phosphate buffer) from equine skeletal muscle (Sigma, St. Louis, MO) was placed in the UV cuvette, and absorbance reading at room temperature was taken. The temperature was then raised to 30 ºC and the absorbance was recorded. After one hour, the absorbance was recorded again. The UV spectrum was retaken after another h. The temperature was increased by another 10 ºC and a spectrum was taken. The absorbance was recorded again after one and two h. This process was continued in temperature increments of 10 ºC until the temperature reached 70 ºC. The myoglobin cuvette then sat at room temperature overnight. The absorbance was recorded. The temperature was then raised directly to 70 ºC. Uv-vis spectra were taken after about five minutes and again after 1 h.

SiaA thermal denaturation: Initial practice on myoglobin. Myoglobin was dissolved in the 50 mM pH 7.5 M buffer (discussed above under the nickel affinity column) to give an OD_{409} of approximately 0.1 and the pH adjusted down to 7.1 by adding dilute HCl. The height of the sample inside the cuvette was measured.

Using the ADL shell of the Varian-Cary, the temperature was programmed to start at 25 °C and end at 95 °C. A 5 min equilibration time was added at the start of the run. The temperature was increased at 0.5 °C per min with a signal averaging time of 0.5 sec. The wavelength was 409 nm. When temperature reached 95 °C, the sample was removed and a blank buffer solution was re-measured. The sample was allowed to cool down to room temperature. The absorbance was re-recorded from 250 to 700 nm. The sample pH and its height were re-measured.

Results and Discussion:

Homologous structure. The sequence of wild type SiaA (Figure 6) was submitted to 3D-JIGSAW, which searches the Protein Database (PDB) for homologous proteins. BtuF (1N4D) was returned by the program at the most homologous structure (Figure 7). The hypothetical 3D structure of wild type SiaA was created and allowed us to see the possible heme ligands included Met79, Tyr63, Tyr179, and His229. The LOOPP program gave three homologous structures, BtuF, CeuE, and FhuD (Figures 8, 9, and 10). In all three cases, Met79 and His229 were in position to be possible axial ligands. The structure of CeuE threaded into SiaA showed that Met79 and His229 were close to one another, and in excellent positions to bind heme.

Although the results of both JIGSAW and LOOPP did not included IsdE as a homologous structure, position specific iterative Blast (PSI-Blast) and pattern hit initiated Blast (PHI-Blast) both yielded IsdE at the most homologous structure to SiaA (Figure 11). SiaA and IsdeE sequences had 45% identical amino acids, 68% positives, and 0% gaps. PSI-Blast and PHI-Blast showed that BtuF, FhuD, and CeuE had 20%, 25%, and 22% identities, and 45%, 43%, 42% positives, and 2%, 11%, 8% gaps, respectively, with the SiaA sequence.

Homology modeling indicates that SiaA is made up mostly of α-helices. From the homology modeling (Figure 7), it can be seen that Tyr179, Tyr63, His229, and Met79 are all possible ligands. We have proposed that SiaA binds heme through the axial ligands His229 and Met79. It is also possible that histidine alone binds the heme. The related Gram negative ShuT protein uses one tyrosine as an axial ligand, and has

significant interaction with the second (Eakanunkul et al, 2005) so these are also possibilities. Three additional axial ligand possibilities are Met/ Met, His/Tyr, and Tyr/Tyr. However, few proteins containing Met/Met and His/Tyr axial ligands are known, and there are no known proteins containing Tyr/Tyr (Dixon, unpublished). Although His/His is a common ligand set, the two histidines are on the same side of the heme in the homology modeling, and are thus not in position to both be axial ligands simultaneously

Growth and isolation of H229A SiaA. Two fermentation runs (2 L and 3 L) of H229A SiaA plasmid in *E. coli* were performed. The 2 L fermentation run gave approximately 9 g of cell pellets after centrifugation. The cell pellets were lysed using a French press. A sample of 90 mL was collected and concentrated to 35 mL for purification by nickel affinity FPLC.

Figure 12 shows the nickel affinity chromatogram. Fractions 1 to 9 are run through. Fractions 15 to 24 show three peaks. Fractions 25 to 31 show one peak.

The UV spectra were taken for fractions 4, 6, 16, 17, 18, 21, 23, 25, 27, and 28 (Figure 13). Fractions 4 and 6 showed very strong bands at 280, indicating substantial concentrations of protein in the flow through. No heme bands were seen as shown by the absence of spectral intensity in the Soret region. The spectra of fractions 16, 17, 18, 21, 23 had shoulders at 420 nm, indicating the presence of heme proteins. The spectra of fractions 25, 27, and 28 had peaks at 420 nm, indicating higher concentrations of holoprotein.

SDS-PAGE (not shown) of fractions 4, 6, 16, 17, 18, 21, 23, 25, 27, and 28 was carried out. Fractions 4 and 6 showed clusters of bands. Fractions 16, 17, 18, 21, and 23 show many separated bands. Fractions 25, 27, and 29 show one strong band, with a molecular weight appropriate for SiaA (Figure 14). Fractions 25 to 31 were combined and exchanged into 10 mM Tris buffer, pH 8.0 to give a final sample of 4.5 mL.

Anion exchange purification was performed on this sample (Figures 15 and 16). A series of 27 fractions were taken, with increasing concentrations of NaCl starting at fraction 15. Three small peaks were seen. The computer reset itself after peak 27. Figure 15 shows the subsequent fractions (labeling old fraction 28 as new fraction 1). Again, three components were seen, eluting at 0.70 to 0.83 M NaCl. Samples were colorless.

SDS-PAGE (not shown) of fractions 21, 22, 23, and 25 of the first chromatogram and 7, 9, 10, and 11 of the second chromatogram was performed. No bands were seen. All fractions were lost.

In the 3 L fermentation run, approximately 10 mL of cell pellets were collected after centrifugation. The cell pellets were lysed using a French press and the eluate was constantly kept on ice to prevent cleavage. A sample of 90 mL was collected; 45 mL was used for purification by nickel affinity FPLC.

Figure 17 shows the nickel affinity chromatogram. Fractions 16 to 36 were collected. Fractions 17 to 22 and 28 to 33 were colorless while fractions 23 – 27 were a cloudy yellowish color. Fractions 16 to 27 showed one major peak while fraction 28 to 33 showed a smaller peak.

The UV spectra were taken for fractions 17 to 22 (Figure 18) and 27 to 33 (Figure 19). All fractions showed bands at 280 and 420, indicating the presence of some apo- and some holoprotein. The peak at 280 nm was larger than that at 420 nm indicating that these were a mixture of apo- and holoprotein [pure holoprotein has a 420/280 ratio of approximately 1.67 (Sook, unpublished)]. Figure 18 shows that the 420/280 nm ratio of all the fractions was approximately 0.2-0.3, indicating that apo- and holoproteins were not separating on the column.

A SDS-PAGE of the French pressed sample before chromatography and fractions 18, 19, 22 to 26, and 27 to 35 of the nickel affinity column was carried out (Figure 20 and 21). The French pressed sample showed a cluster of bands, indicating the presence of multiple proteins. Fractions 18, 19, 22, and 24 also showed clusters of bands. Fractions 23 to 28 showed many separated lighter bands. Fractions 29 and 30 showed two bands with that at the approximate molecular weight of the SiaA far darker than the low molecular weight band. Fractions 31 to 32 showed one strong band while fractions 33 to 35 showed one lighter band.

From the SDS-PAGE, fractions 32 and 33 of the nickel affinity purification appeared to be pure (Figure 22). Fraction 32 and 33 were selected for mass spectrometry. The material was stored in the -80 ^{o}C freezer.

Mass spectrometry. Initial MALDI and ESI mass spectra of fraction 32 had a mass of 35441 Da. However, the spectrum had a number of peaks and was very noisy, indicating substantial salt in the sample (Figures 23 and 24). The expected mass of the protein is 35421 Da (Figures 25, 26, and 27). Thus, the experimental peak was within 20 Da of the

theoretical expectation (0.056%). For MALDI, it is expected that the mass error will be less than 0.05% (18 Da in this instance). For ESI it is expected that the mass error will be less than 0.02% (7 Da in this instance). After desalting, the MALDI mass spectrum showed two peaks with molecular weights of 35386.6 Da and 35589.6 Da (Figures 28 and 29). Thus, one peak was too light by 34 Da and the other peak was too heavy by 169 Da. It was not known why desalting gave two peaks with masses that did not match the theoretical mass.

A MALDI mass spectrum for fraction 33 was taken using carbonic anhydrase as an internal standard (Figure 30). The sample had a mass of 35441 Da before desalting and 35527 Da after desalting (Figure 31). Again, the peak appeared at higher mass after desalting.

Before desalting, both fractions 32 and 33 had a mass of 35441 Da, which was heavier than expected by 20 Da. The mass of 35441 is almost within the generally accepted error of 0.05% from the expected mass of 35421 Da. Alternatively, the protein may have bound a sodium ion. We had observed variable numbers of bound sodium ions in previous spectra of SiaA from our laboratory. Replacement of a proton with a sodium ion increases the mass of the protein by 22 Da. If the protein bound a sodium ion, the experimental and theoretical masses were very close (35441 – Na = 35419 and 35421, respectively).

Calculation of holoprotein. The experimental ratio of the peak at 409 nm to that at 280 nm was 0.25 ± 0.04, showing that the apo- and holoprotein did not separate on the column (Figure 32). Approximately 15% of the protein was found in the holo form.

Assuming an extinction coefficient of 1 x 10^5 M^{-1} cm^{-1} for the holoprotein at the Soret, 0.88 mg of holoprotein was isolated, indicating that the total amount isolated was 5.9 mg.

SiaA temperature stability. Studies of the temperature stability of SiaA were planned. An initial practice run was performed with myoglobin to test the protocol (Figure 33 and 34). The UV-vis spectrum showed two peaks, at 280 (apo- and holoprotein) and 420 (holoprotein) nm. Myoglobin was stable up to 60 ℃ (Figure 33). The protein started to denature, as shown by the shift in the position and intensity of the heme band, when the temperature reached 70 ℃ (Figure 34).

SiaA thermal denaturation. To test the non-linear curve fitting program, the following procedure was followed. First, a theoretical data set was created in Excel by assigning numbers for the folded absorbance, folded slope, unfolded absorbance, unfolded slope, enthalpy, and melting temperature. The expected extent of unfolding was calculated as a function of temperature (Figure 35). These theoretical values were then fitted using Kaleidagraph and the same equation. In general, one person created the theoretical data and a second person fit the data.

Kaleidagraph fitted values for all variables were then compared with theoretical values. Several trials and errors were carried out until Kaleidagraph values and theoretical values matched. These trials helped solve programming errors.

It was desired to run a thermal denaturation of H229A SiaA. This sample was 15% holoprotein and 85% apo-protein. When the experiment was attempted, an increase, rather than a decrease in absorbance was observed. The sample after heating was opaque.

It was assumed that the apoprotein had denatured, leading to the opaqueness of the sample.

It was hoped that it would be possible to perform a thermal denaturation of SiaA, even with a substantial fraction of apoprotein, if the experiment could be done at a very low absorbance of the holoprotein. It was desired to test a sample with an absorbance of 0.1 at 409 nm. A concentrated myoglobin sample was prepared with an OD_{409} of 1.041 (Figure 36). Appropriate dilutions gave a sample with an OD_{409} of 0.109 (Figure 34).

Denaturation was run by heating the sample from at 25 °C to 95 °C at 0.5 °C per min (Figure 37). The sample had the pH 7.11 and a height of 3.5 cm before denaturation and pH 7.19 and a height of 2.7 cm after denaturation. Over the course of the experiment, the height of the sample decreased 0.8 cm and the pH increased by 0.09. The sample had OD_{409} of 0.187 after denaturation (Figure 38). Evaporation of the sample presumably led to an increase in concentration by a factor of 1.29. This increase in concentration was presumably not linear over the course of the experiment, and therefore was not taken into account in the data fitting.

Non-linear least squares fitting of the data to the relevant equation (Figure 35) was performed with Kaleidagraph. Initially, one makes estimates of values for the six relevant variables. These were, y_n (m1) = 0.9, m_n (m2) = -0.0001518 abs/°C, y_u (m3) = 0.02125, m_u (m4) = 0.0001086 abs/°C, ΔH (m5) = 10000 J, and T_m (m6) = 78 °C. A series of input parameters with numerical values near these initial estimates were tried. The final 10 fitting runs are shown in Figure 39. Various different sets of initial values gave very similar sets of fitted parameters (Figure 40). The final error for each variable was less than 1%. The melting point was 78.8 ± 0.1 °C and ΔH was 4611 ± 41 J. The

melting point was consistent with previous findings of 75 °C by the Hildebrand group (Hildebrand et al., 1995).

Conclusions

In this work, the H229 mutant of the heme binding protein SiaA was isolated. Growth of the organism, followed by French press to lyse the cells, and nickel affinity FPLC, gave the desired protein. SDS-PAGE showed that pure H229A was isolated. Both ESI and MALDI mass spectrometry indicated a mass of 35441 Da, very close to the expected value of 35421 Da. The protein may bind a sodium ion in the gas phase. Histidine 229 is likely to be an axial ligand in wild type SiaA; the mutant readily lost heme as evidenced by UV-visible spectra. Calculations indicated that the protein was about 15% holo and 85% apo as isolated. The assignment of H229 as the axial ligand is also consistent with computer threading studies of the structure with related proteins which bind heme, vitamin B_{12} and iron. Preliminary studies on thermal denaturation of heme proteins were performed.

Reference List

Arnoux, P., Haser, R., Izadi, N., Lecroisey, A., Delepierre, M., Wandersman, C., and Czjzek, M. (1999). The crystal structure of HasA, a hemophore secreted by *Serratia marcescens*. *Nature Structural Biology* **6**, 516-520.

Bates, C. S., Montanez, G. E., Woods, C. R., Vincent, R. M., and Eichenbaum, Z. (2003). Identification and characterization of a *Streptococcus pyogenes* operon involved in binding of hemoproteins and acquisition of iron. *Infection and Immunity* **71**, 1042-1055.

Bates, C. S., Toukoki, C., Neely, M. N., and Eichenbaum, Z. (2005). Characterization of MtsR, a new metal regulator in group A streptococcus, involved in iron acquisition and virulence. *Infection and Immunity* **73**, 5743-5753.

Borths, E. L., Locher, K. P., Lee, A. T., and Rees, D. C. (2002). The structure of *Escherichia coli* BtuF and binding to its cognate ATP binding cassette transporter. *Proceedings of the National Academy of Sciences of the United States of America* **99**, 16642-16647.

Carter, D. M., Miousse, I. R., Gagnon, J. N., Martinez, E., Clements, A., Lee, J., Hancock, M. A., Gagnon, H., Pawelek, P. D., and Coulton, J. W. (2006). Interactions between TonB from *Escherichia coli* and the periplasmic protein FhuD. *J.Biol.Chem.* **281**, 35413-35424.

Clarke, T. E., Braun, V., Winkelmann, G., Tari, L. W., and Vogel, H. J. (2002a). X-ray crystallographic structures of the *Escherichia coli* periplasmic protein FhuD bound to hydroxamate-type siderophores and the antibiotic albomycin. *Journal of Biological Chemistry* **277**, 13966-13972.

Clarke, T. E., Rohrbach, M. R., Tari, L. W., Vogel, H. J., and Koster, W. (2002b). Ferric hydroxamate binding protein FhuD from *Escherichia coli*: Mutants in conserved and non-conserved regions. *Biometals* **15**, 121-131.

Crosa, J. H., Mey, A. R., and Payne, S. M. (2004). "Iron Transport in Bacteria." ASM Press, Washington, DC.

Cunningham, M. W. (2000). Pathogenesis of group A streptococcal infections. *Clinical Microbiology Reviews* **13**, 470-511.

Deniau, C., Couprie, J., Simenel, C., Kumar, V., Stojiljkovic, I., Wandersman, C., Delepierre, M., and Lecroisey, A. (2001). H-1, N-15 and C-13 resonance assignments for the gallium protoporphyrin IX-HasA(sm) hemophore complex. *Journal of Biomolecular NMR* **21**, 189-190.

Deniau, C., Gilli, R., Izadi-Pruneyre, N., Létoffé, S., Delepierre, M., Wandersman, C., Briand, C., and Lecroisey, A. (2003). Thermodynamics of heme binding to the

HasA(SM) hemophore: Effect of mutations at three key residues for heme uptake. *Biochemistry.* **42**, 10627-10633.

Eakanunkul, S., Lukat-Rodgers, G. S., Sumithran, S., Ghosh, A., Rodgers, K. R., Dawson, J. H., and Wilks, A. (2005). Characterization of the periplasmic heme-binding protein ShuT from the heme uptake system of *Shigella dysenteriae*. *Biochemistry.* **44**, 13179-13191.

Eichenbaum, Z., Green, B. D., and Scott, J. R. (1996a). Iron starvation causes release from the group A streptococcus of the ADP-ribosylating protein called plasmin receptor or surface glyceraldehyde-3-phosphate-dehydrogenase. *Infection and Immunity* **64**, 1956-1960.

Eichenbaum, Z., Muller, E., Morse, S. A., and Scott, J. R. (1996b). Acquisition of iron from host proteins by the group A *Streptococcus*. *Infection and Immunity* **64**, 5428-5429.

Higgins, C. F. (1992). ABC Transporters - from Microorganisms to Man. *Annual Review of Cell Biology* **8**, 67-113.

Higgins, C. F. (2001). ABC transporters: physiology, structure and mechanism--an overview. *Res.Microbiol.* **152**, 205-210.

Higgins, C. F. and Linton, K. J. (2001). Structural biology. The xyz of ABC transporters. *Science* **293**, 1782-1784.

Hildebrand, D. P., Burk, D. L., Maurus, R., Ferrer, J. C., Brayer, G. D., and Mauk, A. G. (1995). The proximal ligand variant His93Tyr of horse heart myoglobin. *Biochemistry.* **34**, 1997-2005.

Jones, P. M. and George, A. M. (2004). The ABC transporter structure and mechanism: Perspectives on recent research. *Cell Mol.Life Sci.* **61**, 682-699.

Jones, P. M. and George, A. M. (2005). Multidrug resistance in parasites: ABC transporters, P-glycoproteins and molecular modelling. *Int.J.Parasitol.* **35**, 555-566.

Jonsson, I. M., Mazmanian, S. K., Schneewind, O., Bremell, T., and Tarkowski, A. (2003). The role of *Staphylococcus aureus* sortase A and sortase B in murine arthritis. *Microbes and Infection* **5**, 775-780.

Karpowich, N. K., Huang, H. H., Smith, P. C., and Hunt, J. F. (2003). Crystal structures of the BtuF periplasmic-binding protein for vitamin B12 suggest a functionally important reduction in protein mobility upon ligand binding. *Journal of Biological Chemistry* **278**, 8429-8434.

Krewulak, K. D., Shepherd, C. M., and Vogel, H. J. (2005). Molecular dynamics simulations of the periplasmic ferric-hydroxamate binding protein FhuD. *Biometals* **18**, 375-386.

Lei, B. F., Liu, M. Y., Prater, C. I., Kala, S. V., Deleo, F. R., and Musser, J. M. (2003). Identification and characterization of HtsA, a second heme-binding protein made by *Streptococcus pyogenes*. *Infection and Immunity* **71**, 5962-5969.

Liu, M. and Lei, B. F. (2005). Heme transfer from streptococcal cell surface protein Shp to HtsA of transporter HtsABC. *Infection and Immunity* **73**, 5086-5092.

Locher, K. P. (2004). Structure and mechanism of ABC transporters. *Current Opinion In Structural Biology* **14**, 426-431.

Locher, K. P. and Borths, E. (2004). ABC transporter architecture and mechanism: Implications from the crystal structures of BtuCD and BtuF. *FEBS Lett.* **564**, 264-268.

Maresso, A. W. and Schneewind, O. (2006). Iron acquisition and transport in *Staphylococcus aureus*. *Biometals* **19**, 193-203.

Mazmanian, S. K., Skaar, E. P., Gaspar, A. H., Humayun, M., Gornicki, P., Jelenska, J., Joachmiak, A., Missiakas, D. M., and Schneewind, O. (2003). Passage of heme-iron across the envelope of *Staphylococcus aureus*. *Science* **299**, 906-909.

Muller, A., Wilkinson, A. J., Wilson, K. S., and Duhme-Klair, A. K. (2006). An [{Fe(mecam)}$_{(2)}$]$^{(6-)}$ bridge in the crystal structure of a ferric enterobactin binding protein. *Angew.Chem.Int.Ed.* **45**, 5132-5136.

Paterson, G. K. and Mitchell, T. J. (2004). The biology of Gram-positive sortase enzymes. *Trends in Microbiology* **12**, 89-95.

Raymond, K. N. and Dertz, E. A. (2004). Biochemical and physical properties of siderophores. *In* "Iron Transport in Bacteria" (J. H. Crosa, A. R. Mey, and S. M. Payne, Eds.), pp. 3-17. ASM Press, Washington, DC.

Raymond, K. N., Dertz, E. A., and Kim, S. S. (2003). Enterobactin: An archetype for microbial iron transport. *Proc.Natl.Acad.Sci.USA* **100**, 3584-3588.

Rukhman, V., Anati, R., Melamed-Frank, M., and Adir, N. (2005). The MntC crystal structure suggests that import of Mn^{2+} in cyanobacteria is redox controlled. *Journal Of Molecular Biology* **348**, 961-969.

Skaar, E. P., Gaspar, A. H., and Schneewind, O. (2004). IsdG and IsdI, heme-degrading enzymes in the cytoplasm of *Staphylococcus aureus*. *Journal of Biological Chemistry* **279**, 436-443.

Skaar, E. P. and Schneewind, O. (2004). Iron-regulated surface determinants (Isd) of *Staphylococcus aureus*: stealing iron from heme. *Microbes and Infection* **6**, 390-397.

Swint, L. and Robertson, A. D. (1993). Thermodynamics of unfolding for turkey ovomucoid third domain: Thermal and chemical denaturation. *Protein Sci.* **2**, 2037-2049.

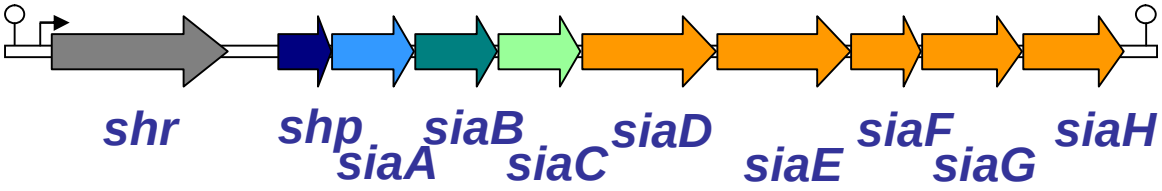

Figure 1. Streptococcal iron acquisition gene cluster.

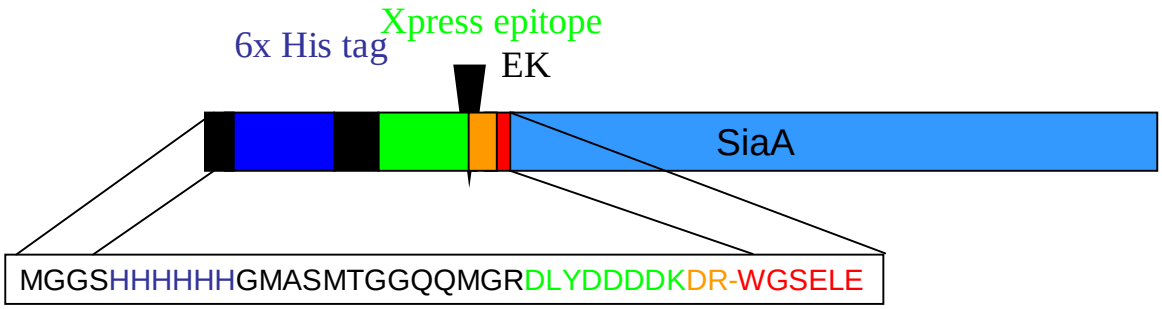

Figure 2. The SiaA construct (Bates et al, 2005). The black band is the lipoprotein that was replaced with His-Tag (blue), Xpress epitope (green), and enterokinase (EK) (green) cleavage site, and additional residues (red). The orange sequence shows the observed alternative EK cleavage site.

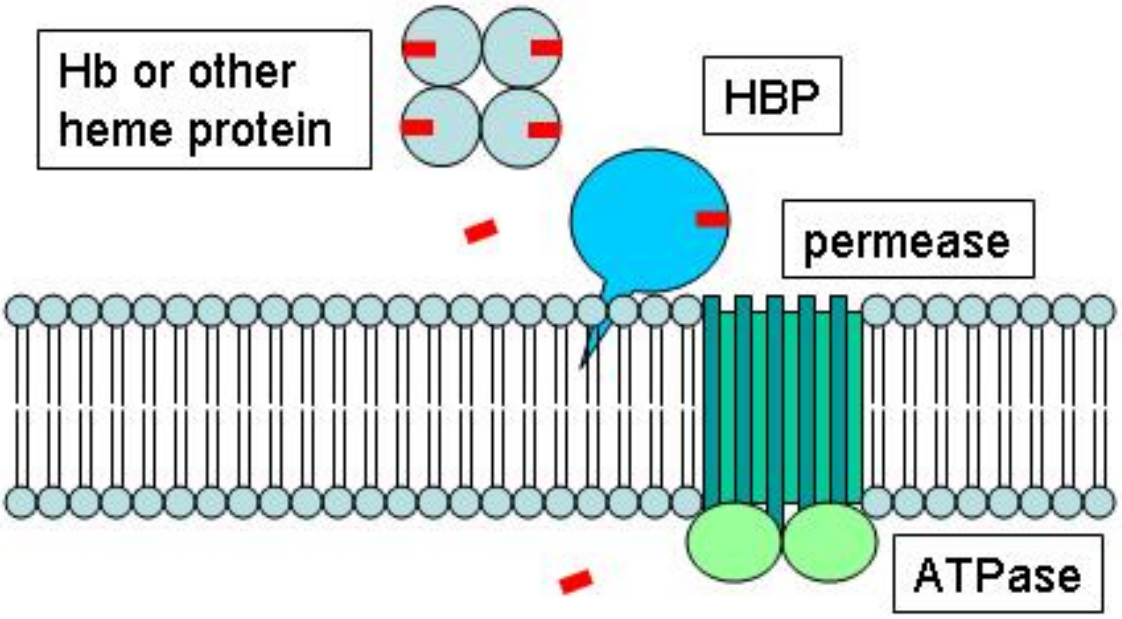

Figure 3. Representative diagram of Sia ABC. SiaA, bound to the plasma membrane, binds heme and carries it to SiaB, the permease, which transports heme to the inner membrane through SiaC, the ATPase system.

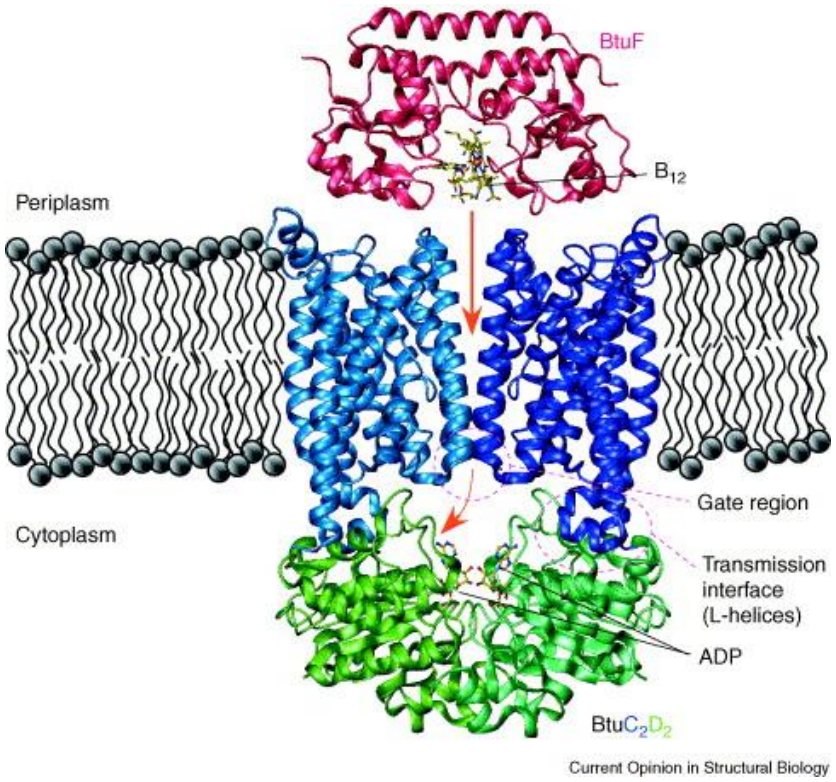

Figure 4. B_{12}-bound BtuF associating with $BtuC_2D_2$. Reprinted from (Locher et al, 2004).

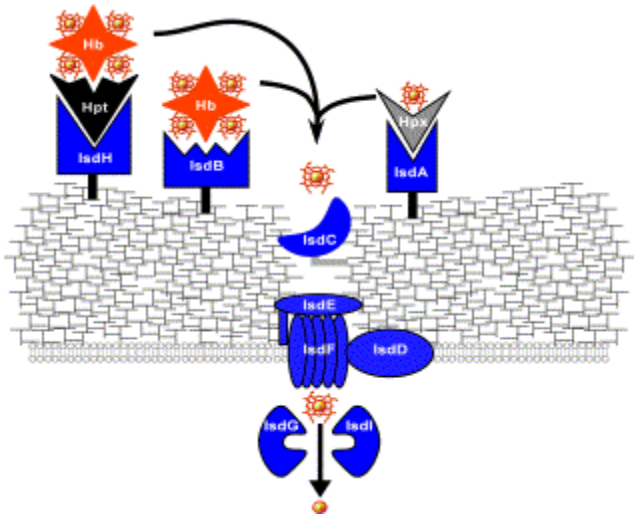

Figure 5. An Isd system model displaying the cell wall linked proteins, IsdABCH, the transporter, IsdDEF, and the cytosolic proteins IsdGH. Reprinted from (Skaar et al, 2004).

1	MIKRCKGIGL	ALMAFFLVAC	VNQHPKTAKE	TEQQRIVATS
41	VAVVDICDRL	NLDLVGVCDS	KLYTLPKRYD	AVKRVGLPMN
81	PDIELIASLK	PTWILSPNSL	QEDLEPKYQK	LDTEYGFLNL
121	RSVEGMYQSI	DDLGNLFQRQ	QEAKELRQQY	QDYYRAFQAK
161	RKGKKKPKVL	ILMGLPGSYL	VATNQSYVGN	LLDLAGGENV
201	YQSDEKEFLS	ANPEDMLAKE	PDLILRTAHA	IPDKVKVMFD
241	KEFAENDIWK	HFTAVKEGKV	YDLDNTLFGM	SAKLNYPEAL
281	DTLTQLFDHV	GDHP		

MGGSHHHHHHGMASMTGGQQMGRDLYDDDDK[DR[WGSELEVNQHPKTAKET
EQQRIVATSVAVVDICDRLNLDLVGVCDSKLYTLPKRYDAVKRVGLPMNPDIELI
ASLKPTWILSPNSLQEDLEPKYQKLDTEYGFLNLRSVEGMYQSIDDLGNLFQRQQ
EAKELRQQYQDYYRAFQAKRKGKKKPKVLILMGLPGSYLVATNQSYVGNLLDL
AGGENVYQSDEKEFLSANPEDMLAKEPDLILRTAHAIPDKVKVMFDKEFAENDI
WKHFTAVKEGKVYDLDNTLFGMSAKLNYPEALDTLTQLFDHVGDHP]]

Figure 6. (Top) The sequence of wild type SiaA (Bates et al, 2005). (Bottom) The recombinant SiaA sequence (Bates et al, 2005). Enterokinase is expected to cleave at the red bracket (after DDDDK). However, experiments showed that EK cleaved at both brackets. The molecular weight of the entire construct is 35,618. Within the red brackets, the apoprotein weighs 31,918 while the holoprotein weighs 32,534. For the black brackets, the apoprotein weighs 32,189 while the holoprotein weighs 32,805. The blue sequence at the N-terminus contains a His-Tag and Xpress epitope.

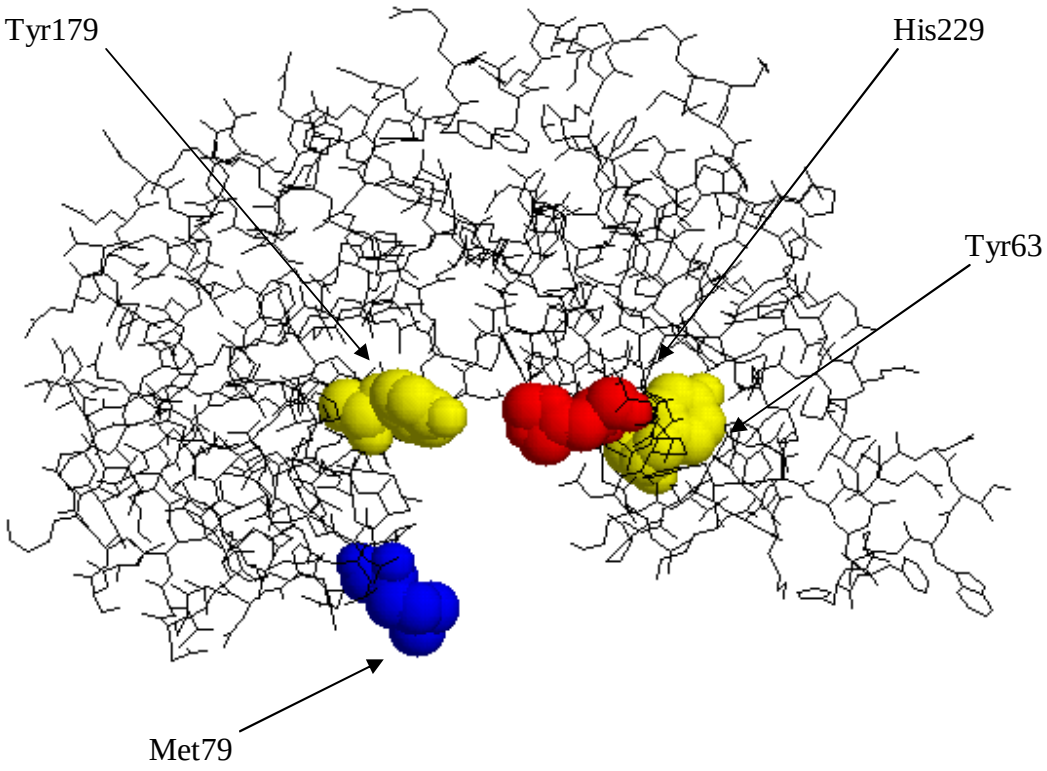

Figure 7. Wild type SiaA was threaded into 1N4D (BtuF ligand unbound) (Karpowich et al, 2003). The His229, Met79, Tyr63, and Tyr179 residues are colored red, blue, yellow and yellow, respectively, and displayed using space filling models. Data are from 3D-Jigsaw, visualized with RasMol 2.7.2.2.1.

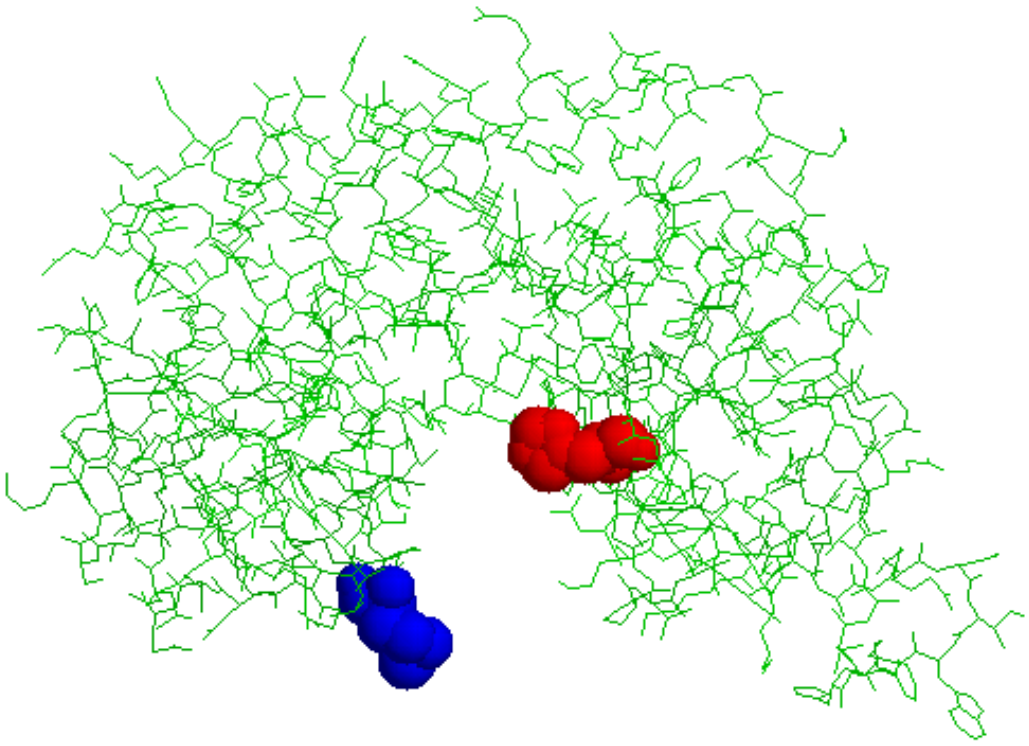

Figure 8. Wild type SiaA was threaded into 1N4A (BtuF ligand unbound) (Karpowich et al, 2003). The proposed His229 and Met79 residues are showed in red and blue, respectively. Data are from LOOPP, visualized with RasMol 2.7.2.2.1.

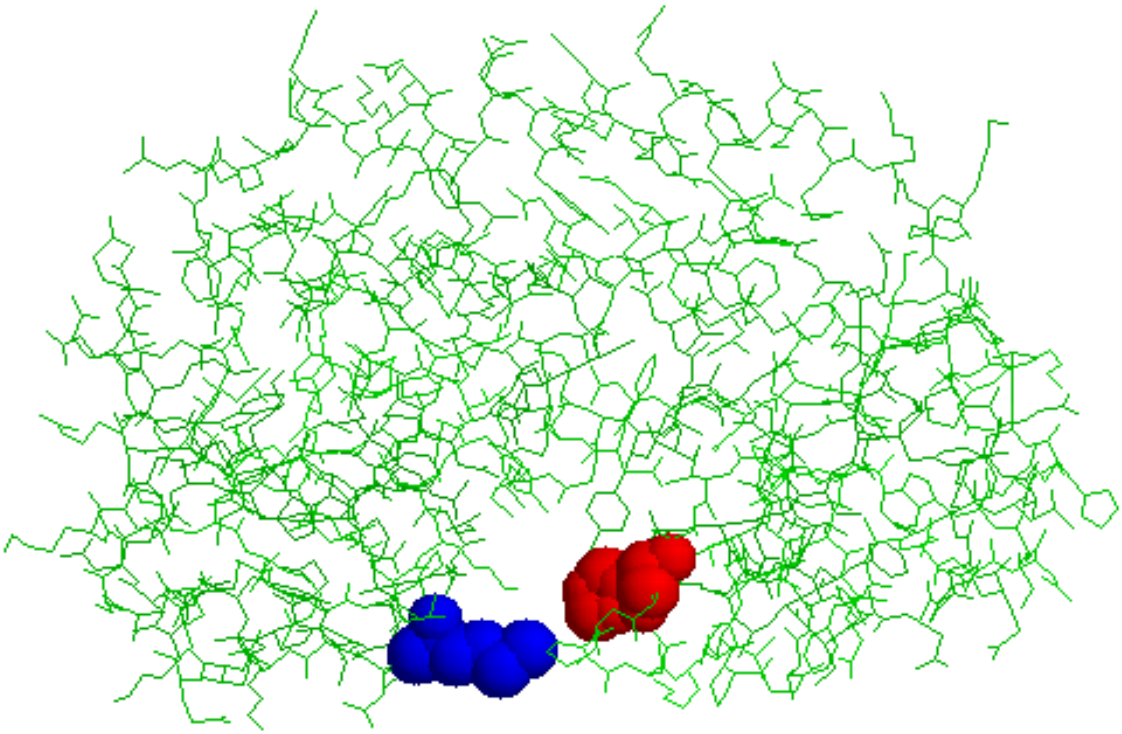

Figure 9. Wild type SiaA was threaded into 2CHU (CeuE ligand unbound) (Muller et al, 2006). The proposed His229 and Met79 residues are showed in red and blue respectively. Data are from LOOPP, visualized with RasMol 2.7.2.2.1.

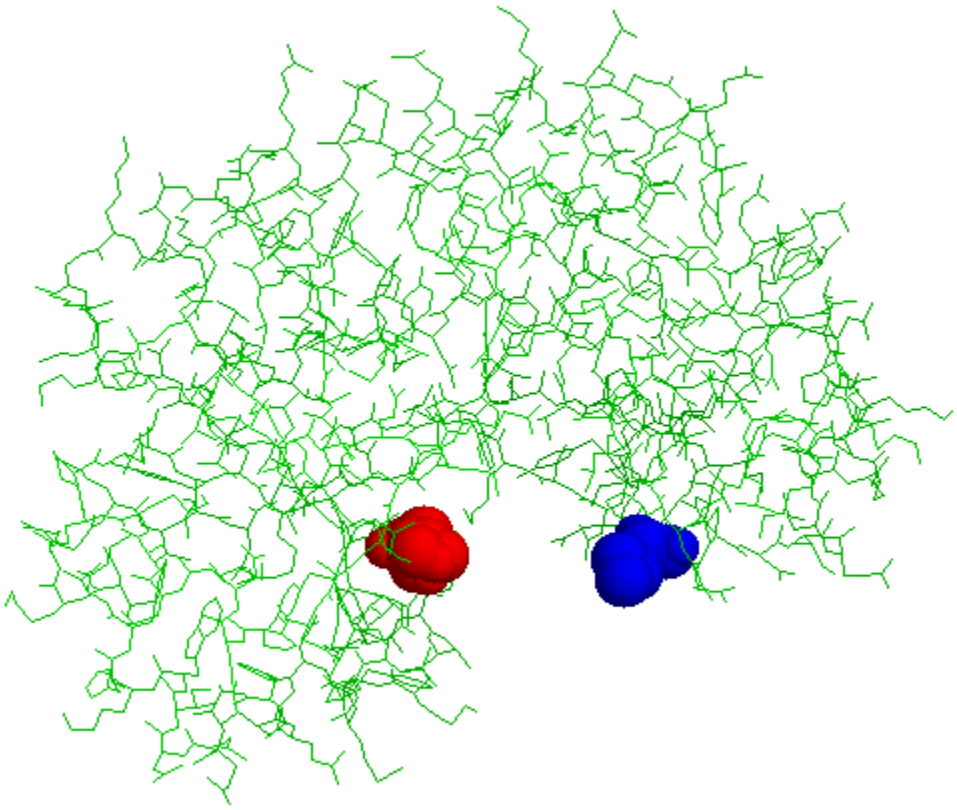

Figure 10. Wild type SiaA was threaded into 1K7S (FhuD ligand unbound) (Clarke et al, 2002a). The proposed His229 and Met79 residues are showed in red and blue respectively. Data are from LOOPP, visualized with RasMol 2.7.2.2.1.

```
SiaA 35  RIVATSVAVVDICDRLNLD--LVGVCDSKLYTL----PKRYDAVKRVGLPMNPDIELIASLKPTWI  94
         RIV T+VA+    D+L+L   +VG   S   TL    P RY  V  +G PM P++E +  LKPT +
IsdE 6   RIVPTTVALTMTLDKLDLP--IVGKPTS-YKTL----PNRYKDVPEIGQPMEPNVEAVKKLKPTHV  64
         R++  S A  ++     +    VGV     Y      P +   +++V      ++E I +LKP  +
BtuF 4   RVITLSPANTELAFAAGIT--PVGVSSYSDY------PPQAQKIEQVSTWQGXNLERIVALKPDLV  61
         RIVA     V++   L +     GV D+  Y L    P   D+V  VGL   P++EL+  +KP+++
FhuD 4   RIVALEWLPVELLLALGIV--PYGVADTINYRLWVSEPPLPDSVIDVGLRTEPNLELLTEMKPSFM  70
         ++V   + ++D  D L L+  +VGV    L        +++     VG     D E I +LKP  I
CeuE 38  KVVILDLGILDTFDALKLNDKVVGVPAKNLPKY----LQQFKNKPSVGGVQQVDFEAINALKPDLI  99
```

PDB ID	Name	Identities (%)	Positives (%)	Gaps (%)
2Q8Q	IsdE	45	68	0
2QI9	BtuF	20	45	2
1EFD	FhuD	25	43	11
2CHU	CeuE	22	42	8

Figure 11. (Top) Sequence alignment between SiaA and IsdE, BtuF, CeuE, and FhuD from PSI-Blast and PHI-Blast. (Bottom) Percent identities, positives, and gaps between SiaA sequence and IsdE, BtuF, FhuD, and CeuE sequences. IsdE has highest percentage of identities, positives, and lowest percentage of gap to SiaA.

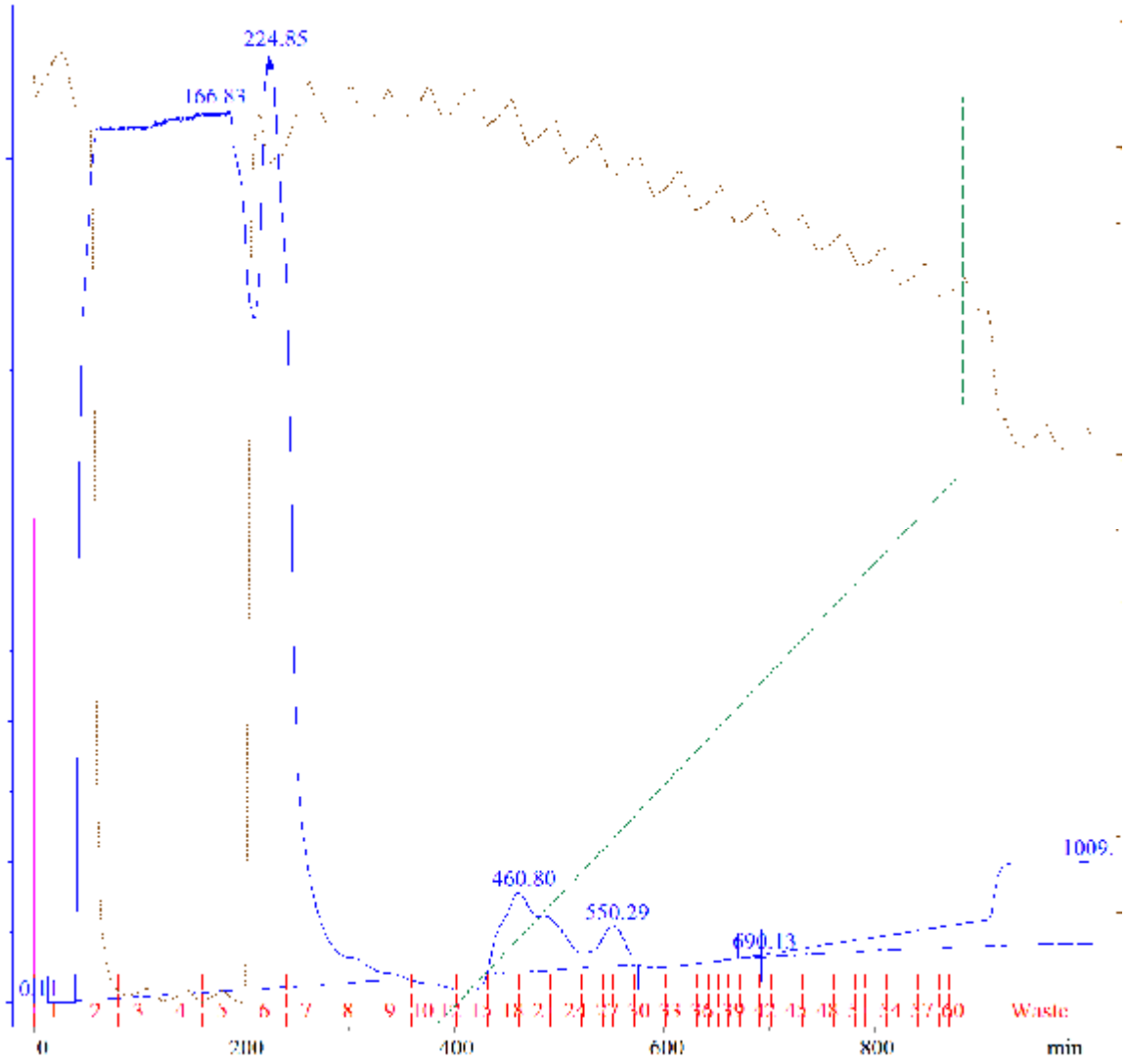

Figure 12. Nickel affinity FPLC chromatogram performed on French pressed, centrifuged, and filtered supernatant from the 2 L run. The dotted line starting at fraction 10 indicates a linearly increasing concentration of elution buffer (binding buffer with 0.5 M imidazole). SiaA elutes at approximately 0.1 M imidazole. Fractions 15-31 were collected.

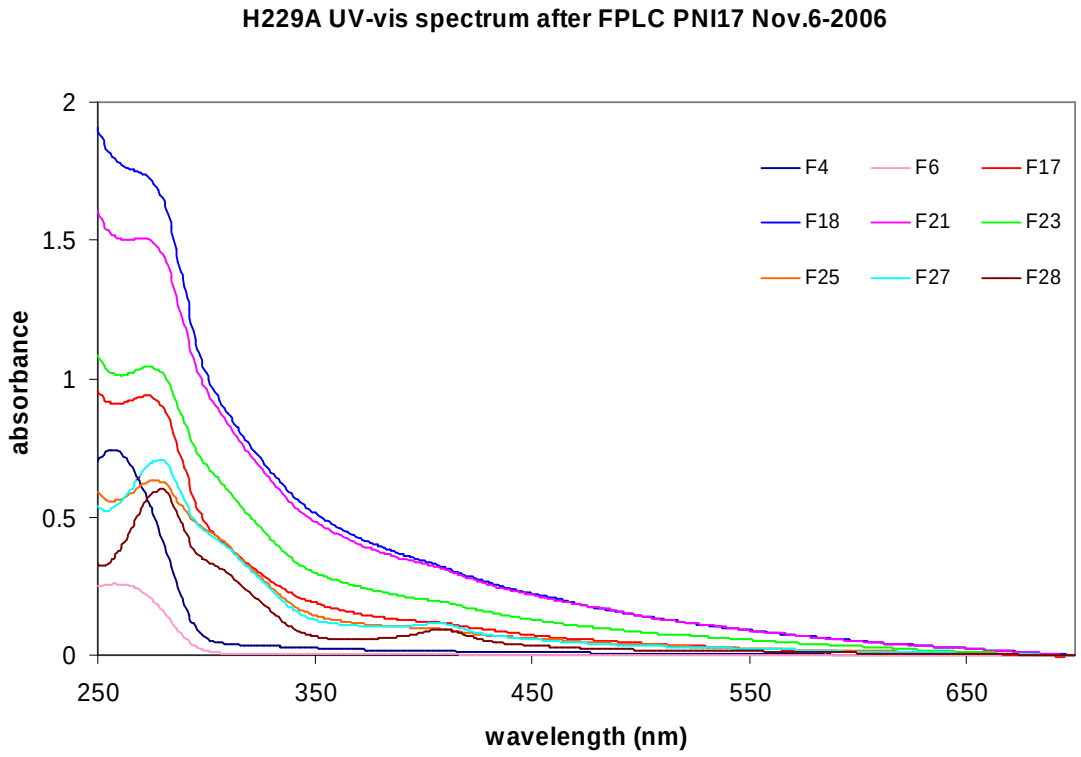

Figure 13. The UV-vis spectra of the fractions from Figure 11. The fraction with the greatest amount of heme (420 nm) appears to be F28, indicating that the last of the peaks eluted is the holoprotein.

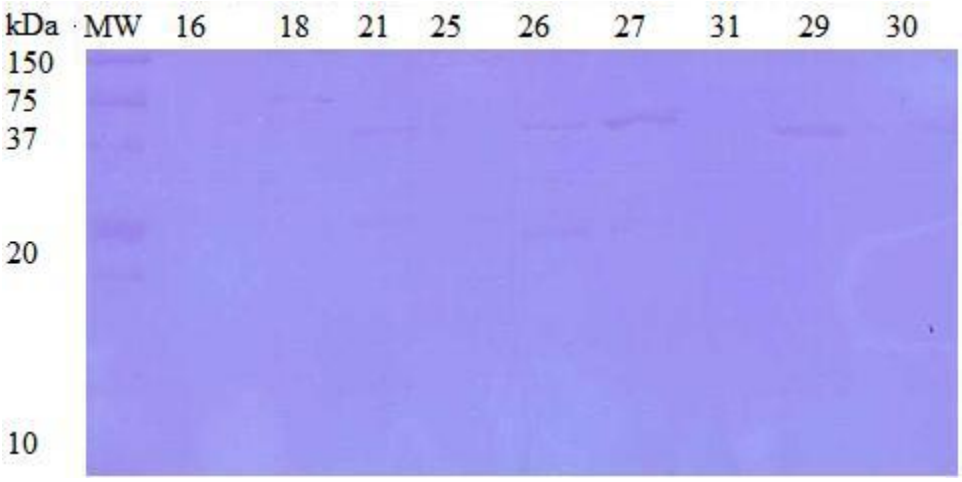

Figure 14. SDS-PAGE of nickel affinity FPLC fractions 16, 18, 21, 25, 26, 27, 29, 30, and 31 from 2 L run (Figure 11). The MW lane contains the Precision Plus Protein® molecular weight marker standard. Fractions 26, 27, and 29 show a solid band at approximately 37 kDa.

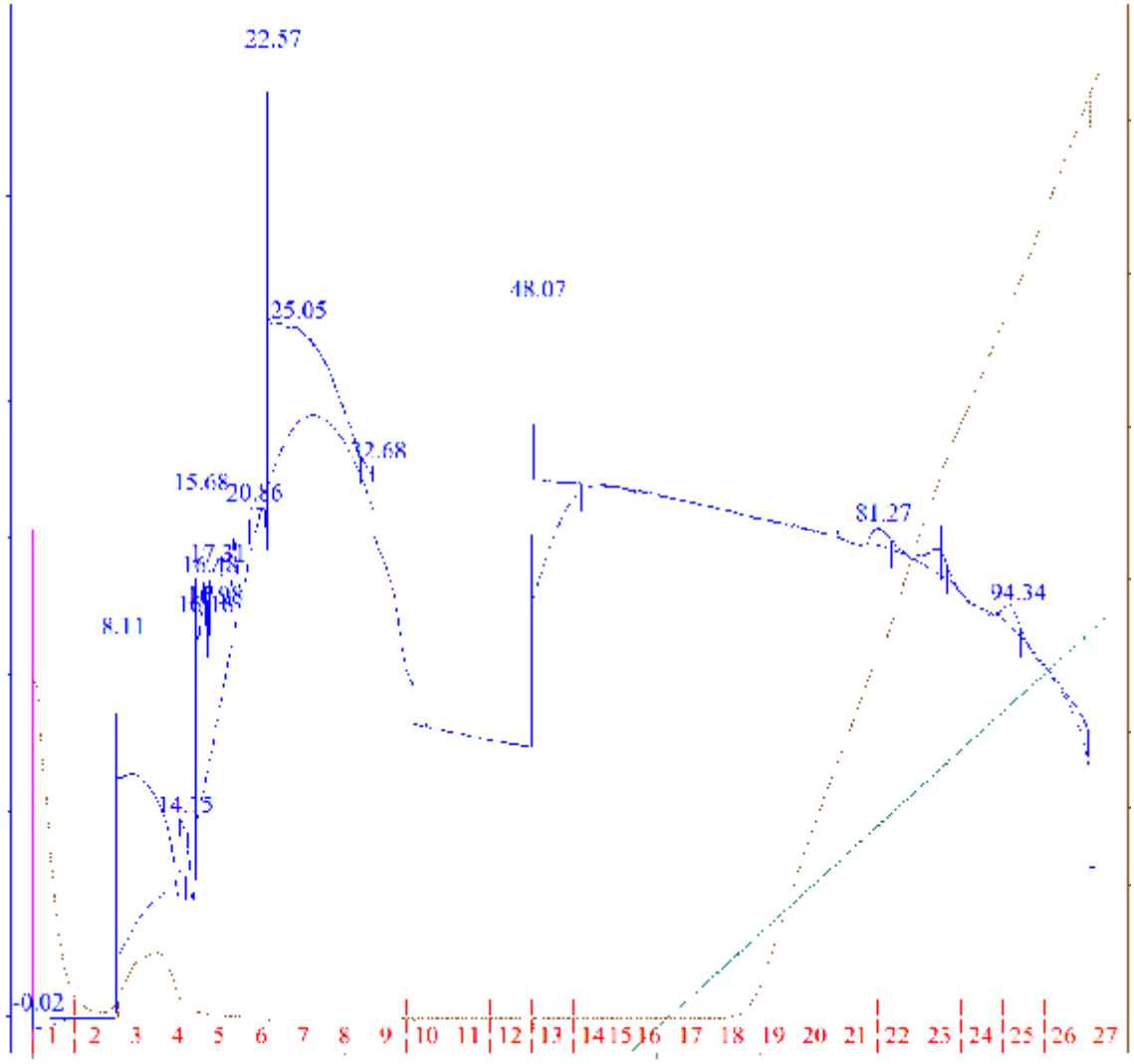

Figure 15. Anion exchange FPLC chromatogram using a HiTrap Q HP (5 mL) column of fractions 25 to 31 from the nickel affinity purification. The green dotted line indicates a linearly increasing concentration of NaCl in the elution buffer. The data was saved in two files, fractions 1-27 and then (renumbering 28 as 1) fractions 1-14 (Figure 15). The elution buffer started at fraction 15. Fractions 21, 23, and 25 (containing the three small peaks) were collected.

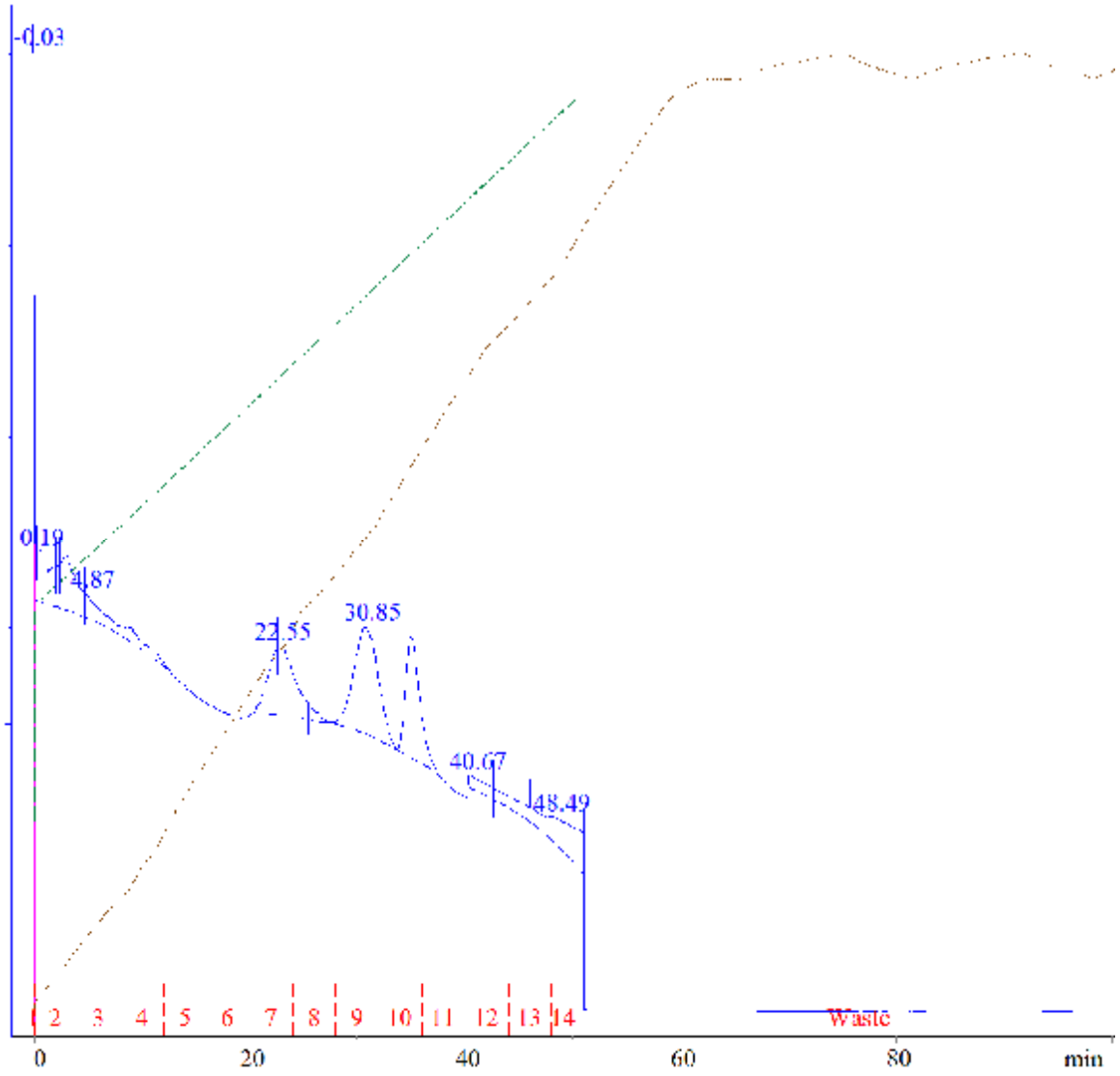

Figure 16. Anion exchange FPLC chromatogram using a HiTrap Q HP (5 mL) column of fractions 25 to 31 from the nickel affinity purification. This is a continuation of data from Figure 14. The green dotted line indicates a linearly increasing concentration of NaCl in the elution buffer. The NaCl concentration at the start of the chromatogram was 0.4 M. The NaCl concentration in the elution buffer was 1.0 M. The peak at 30.85 min eluted at 0.77 M NaCl.

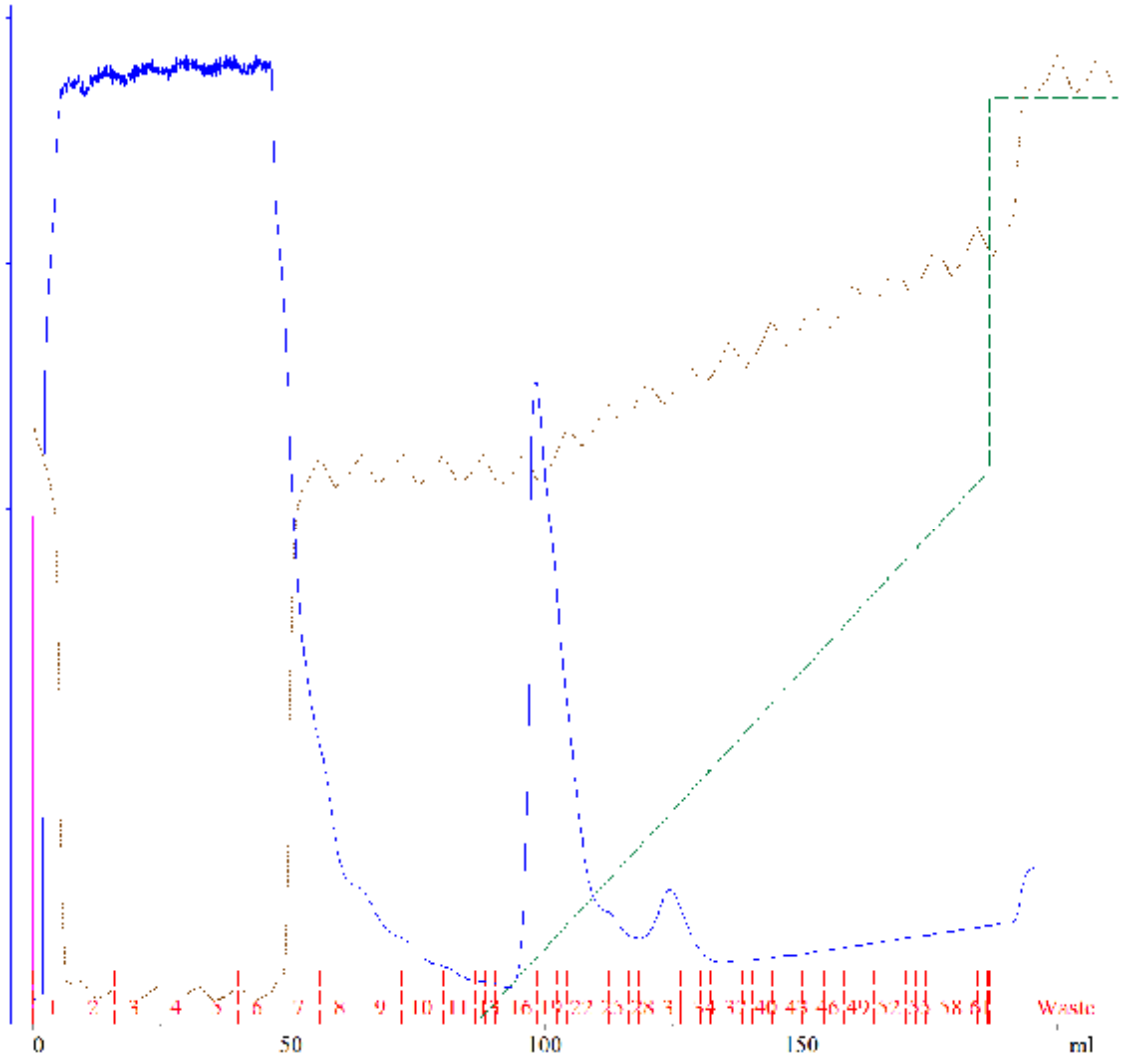

Figure 17. Nickel affinity FPLC chromatogram performed on French pressed, centrifuged, and filtered supernatant from the 3 L run. The dotted line starting at fraction 11 indicates a linearly increasing concentration of elution buffer (binding buffer with 0.5 M imidazole). SiaA is found in fractions 28 – 34. It elutes at approximately 0.12 M imidazole. Fractions 15 - 35 were collected.

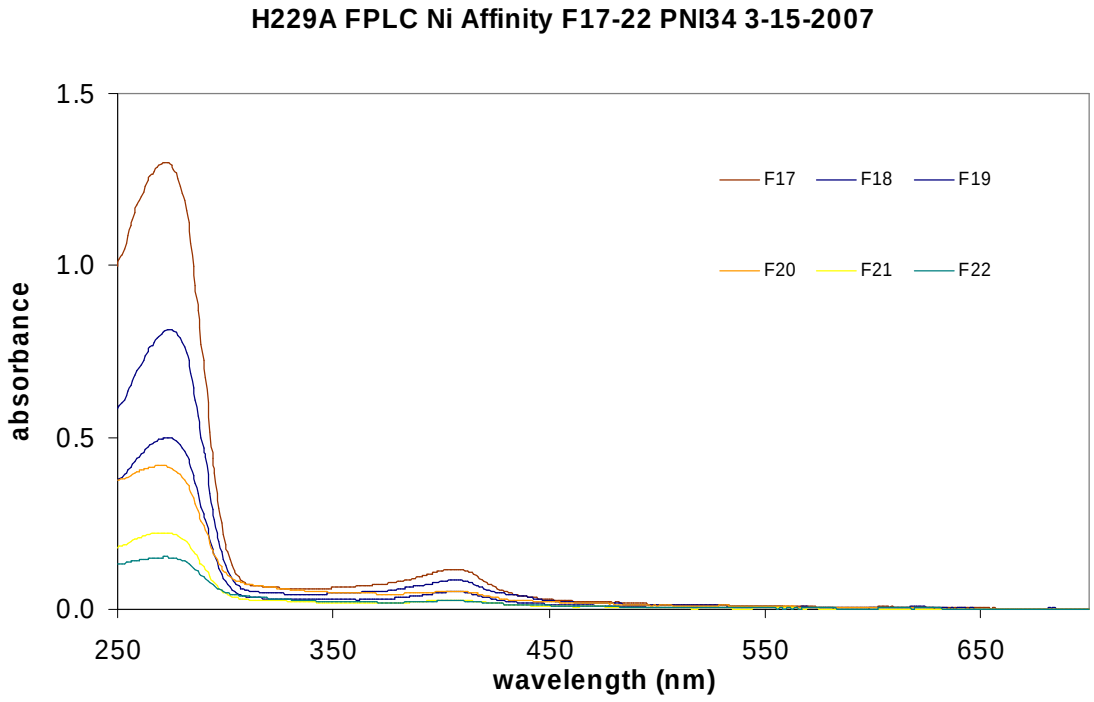

Figure 18. The spectra of fractions 17-22 from the nickel affinity column in Figure 16. The leading edge of the peak has heme; the trailing edge does not appear to contain heme. SDS PAGE (Figure 19) shows that these fractions have a number of proteins.

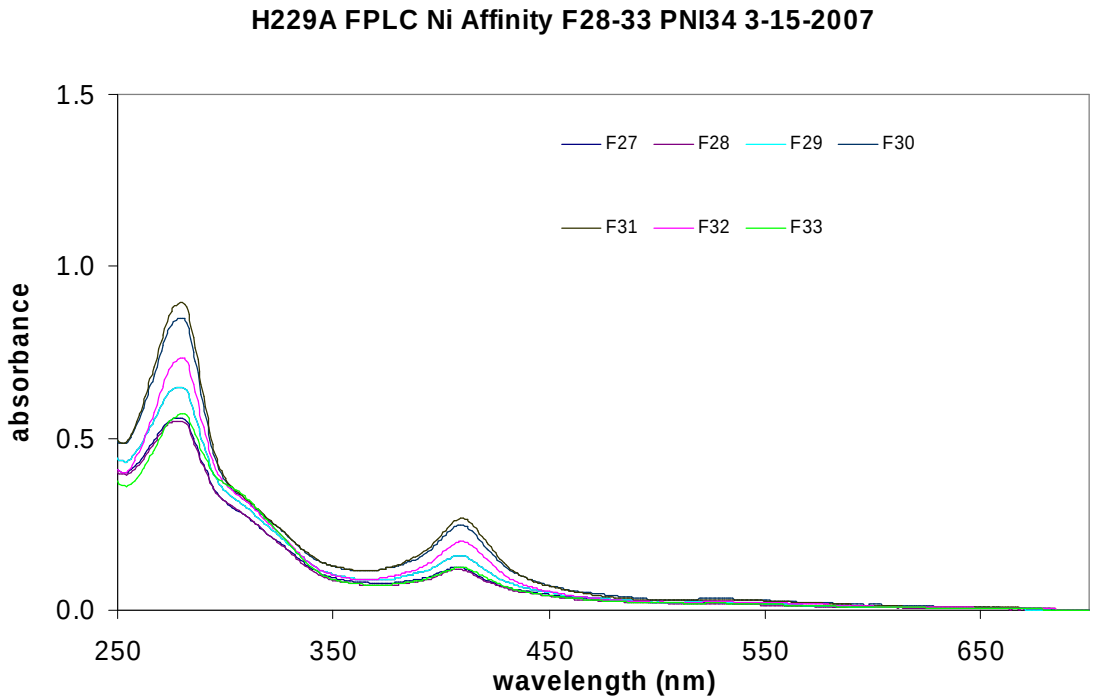

Figure 19. The spectra of fractions 27 – 33. The peaks at 420 nm showed that these fractions contain holoprotein. The fact that the peak at 280 nm is larger than that at 420 nm indicates that these are a mixture of apo- and holoprotein (pure holoprotein has a 420/280 ratio of approximately 1.67 (Sook, unpublished). The fact that the 420/280 ratio of all the fractions is approximately 0.21 to 0.30 indicates that the apo- and holoproteins are not separating on the column.

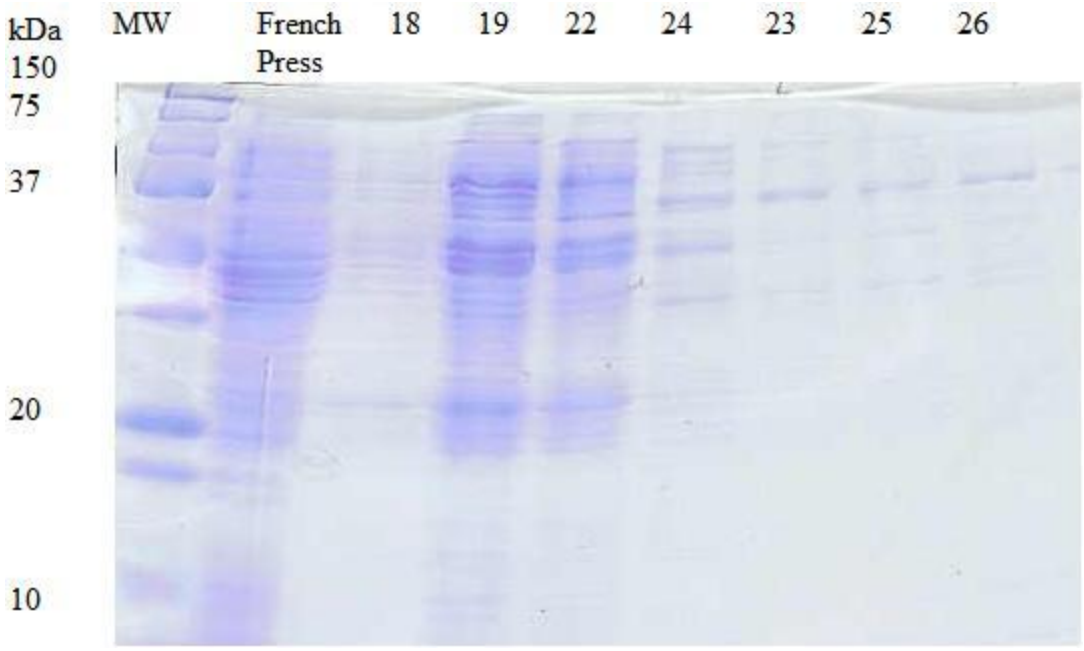

Figure 20. SDS-PAGE of nickel affinity FPLC fractions 18, 19, 22, 23, 24, 25, and 26 from 3 L run (Figure 16). The MW lane contains the Precision Plus Protein® molecular weight marker standard. All fractions contained some contaminant proteins; fractions 23, 25, and 26 are the purest.

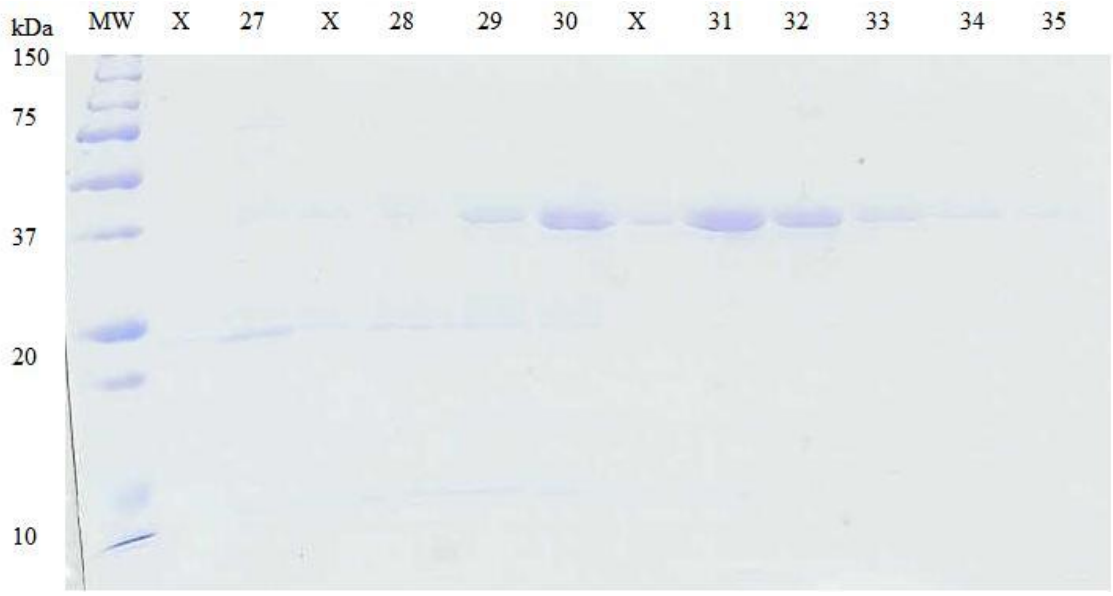

Figure 21. SDS-PAGE of nickel affinity FPLC fractions 27 to 35 from the 3 L run (Figure 16). The MW lane contains the Precision Plus Protein® molecular weight marker standard. Fractions 30, 31, and 32 showed one solid band.

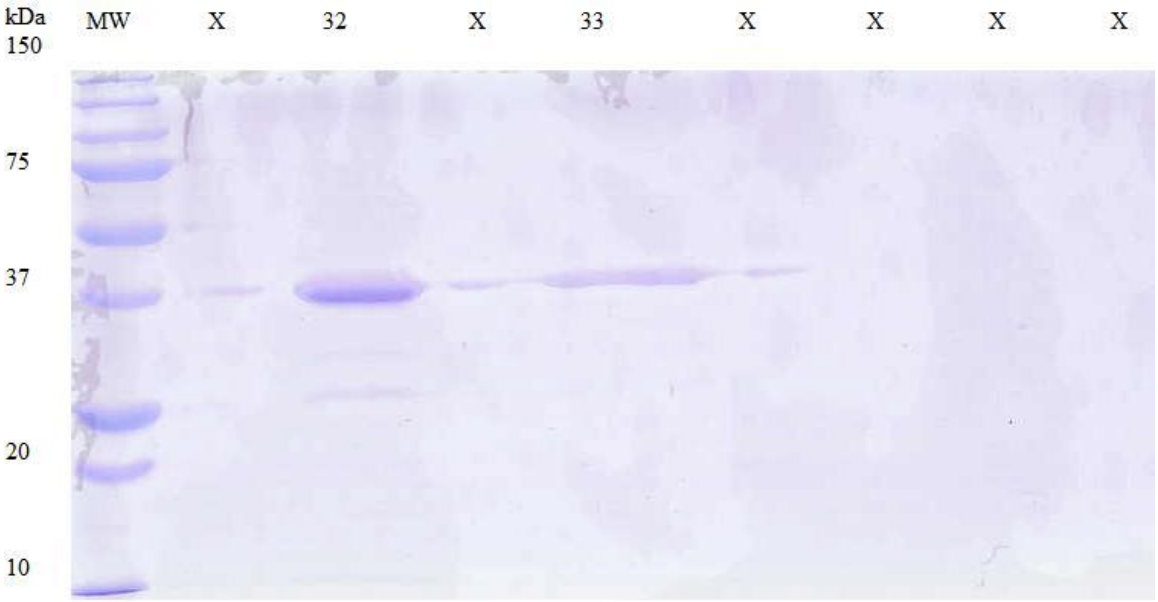

Figure 22. SDS-PAGE of nickel affinity FPLC fractions 32 and 33 from the 3 L run (Figure 16). The MW lane contains the Precision Plus Protein® molecular weight marker standard. Fractions 32 and 33 showed one solid band.

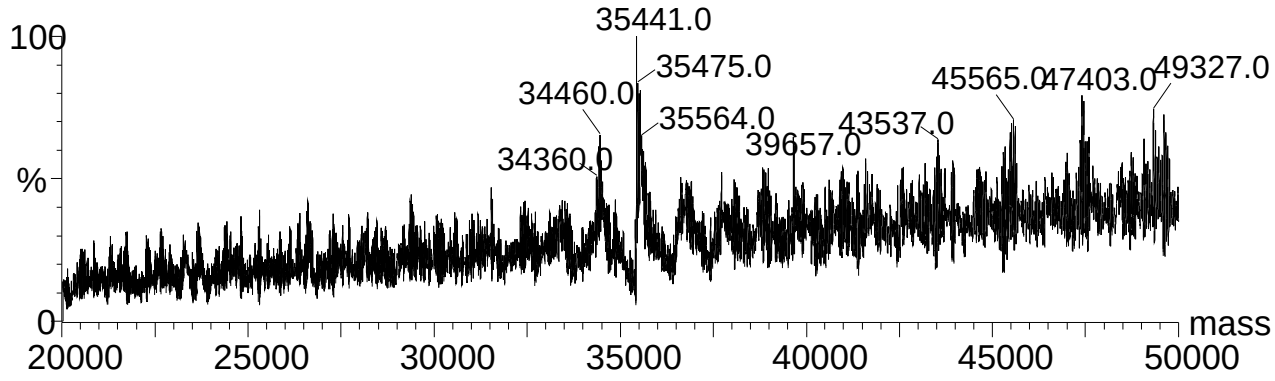

Figure 23. MALDI mass spectrum of fraction 32 from Figure 20. The tallest peak is at 35441 Da. The spectrum indicates that the sample is very salty.

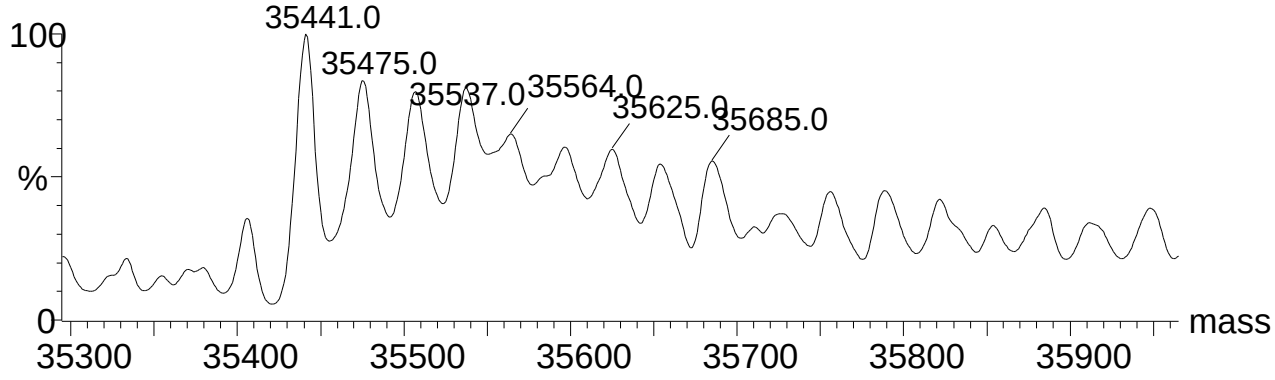

Figure 24. ESI mass spectrometry of fraction 32 from Figure 20. The tallest peak is at 35441.0 Da. The spectrum indicates that the sample is very salty.

Wild type (WT) SiaA Sequence	**Molecular Weight (Da)**
MGGSHHHHHHGMASMTGGQQMGRDLYDDDDK[DR[WGSELEVNQ HPKTAKETEQQRIVATSVAVVDICDRLNLDLVGVCDSKLYTLPKRY DAVKRVGLPMNPDIELIASLKPTWILSPNSLQEDLEPKYQKLDTEYG FLNLRSVEGMYQSIDDLGNLFQRQQEAKELRQQYQDYYRAFQAKR KGKKKPKVLILMGLPGSYLVATNQSYVGNLLDLAGGENVYQSDEK EFLSANPEDMLAKEPDLILRTAHAIPDKVKVMFDKEFAENDIWKHFT AVKEGKVYDLDNTLFGMSAKLNYPEALDTLTQLFDHVGDHP]]	35618.2
_GGSHHHHHHGMASMTGGQQMGRDLYDDDDK[DR[WGSELEVNQ HPKTAKETEQQRIVATSVAVVDICDRLNLDLVGVCDSKLYTLPKRY DAVKRVGLPMNPDIELIASLKPTWILSPNSLQEDLEPKYQKLDTEYG FLNLRSVEGMYQSIDDLGNLFQRQQEAKELRQQYQDYYRAFQAKR KGKKKPKVLILMGLPGSYLVATNQSYVGNLLDLAGGENVYQSDEK EFLSANPEDMLAKEPDLILRTAHAIPDKVKVMFDKEFAENDIWKHFT AVKEGKVYDLDNTLFGMSAKLNYPEALDTLTQLFDHVGDHP]]	35487.0
__GSHHHHHHGMASMTGGQQMGRDLYDDDDK[DR[WGSELEVNQ HPKTAKETEQQRIVATSVAVVDICDRLNLDLVGVCDSKLYTLPKRY DAVKRVGLPMNPDIELIASLKPTWILSPNSLQEDLEPKYQKLDTEYG FLNLRSVEGMYQSIDDLGNLFQRQQEAKELRQQYQDYYRAFQAKR KGKKKPKVLILMGLPGSYLVATNQSYVGNLLDLAGGENVYQSDEK EFLSANPEDMLAKEPDLILRTAHAIPDKVKVMFDKEFAENDIWKHFT AVKEGKVYDLDNTLFGMSAKLNYPEALDTLTQLFDHVGDHP]]	35430.0
MGGSHHHHHHGMASMTGGQQMGRDLYDDDDK[DR[WGSELEVNQ HPKTAKETEQQRIVATSVAVVDICDRLNLDLVGVCDSKLYTLPKRY DAVKRVGLPMNPDIELIASLKPTWILSPNSLQEDLEPKYQKLDTEYG FLNLRSVEGMYQSIDDLGNLFQRQQEAKELRQQYQDYYRAFQAKR KGKKKPKVLILMGLPGSYLVATNQSYVGNLLDLAGGENVYQSDEK EFLSANPEDMLAKEPDLILRTAHAIPDKVKVMFDKEFAENDIWKHFT AVKEGKVYDLDNTLFGMSAKLNYPEALDTLTQLFDHVGDH_]]	35521.1
GGSHHHHHHGMASMTGGQQMGRDLYDDDDK[DR[WGSELEVNQ HPKTAKETEQQRIVATSVAVVDICDRLNLDLVGVCDSKLYTLPKRY DAVKRVGLPMNPDIELIASLKPTWILSPNSLQEDLEPKYQKLDTEYG FLNLRSVEGMYQSIDDLGNLFQRQQEAKELRQQYQDYYRAFQAKR KGKKKPKVLILMGLPGSYLVATNQSYVGNLLDLAGGENVYQSDEK EFLSANPEDMLAKEPDLILRTAHAIPDKVKVMFDKEFAENDIWKHFT AVKEGKVYDLDNTLFGMSAKLNYPEALDTLTQLFDHVGD]]	35389.9

Figure 25: The molecular weight of WT SiaA, SiaA – Met, SiaA – (Met + Gly), SiaA – Pro, and SiaA – (Met + Pro).

Mutant SiaA (H229A) Sequence	**Molecular Weight (Da)**
MGGSHHHHHHGMASMTGGQQMGRDLYDDDDK[DR[WGSELEVNQ HPKTAKETEQQRIVATSVAVVDICDRLNLDLVGVCDSKLYTLPKRYD AVKRVGLPMNPDIELIASLKPTWILSPNSLQEDLEPKYQKLDTEYGFL NLRSVEGMYQSIDDLGNLFQRQQEAKELRQQYQDYYRAFQAKRKGK KKPKVLILMGLPGSYLVATNQSYVGNLLDLAGGENVYQSDEKEFLSA NPEDMLAKEPDLILRTAHAIPDKVKVMFDKEFAENDIWKHFTAVKEG KVYDLDNTLFGMSAKLNYPEALDTLTQLFDHVGD**A**P]]	35552.2
_GGSHHHHHHGMASMTGGQQMGRDLYDDDDK[DR[WGSELEVNQH PKTAKETEQQRIVATSVAVVDICDRLNLDLVGVCDSKLYTLPKRYDA VKRVGLPMNPDIELIASLKPTWILSPNSLQEDLEPKYQKLDTEYGFLN LRSVEGMYQSIDDLGNLFQRQQEAKELRQQYQDYYRAFQAKRKGKK KPKVLILMGLPGSYLVATNQSYVGNLLDLAGGENVYQSDEKEFLSAN PEDMLAKEPDLILRTAHAIPDKVKVMFDKEFAENDIWKHFTAVKEGK VYDLDNTLFGMSAKLNYPEALDTLTQLFDHVGD**A**P]]	35421.0
__GSHHHHHHGMASMTGGQQMGRDLYDDDDK[DR[WGSELEVNQH PKTAKETEQQRIVATSVAVVDICDRLNLDLVGVCDSKLYTLPKRYDA VKRVGLPMNPDIELIASLKPTWILSPNSLQEDLEPKYQKLDTEYGFLN LRSVEGMYQSIDDLGNLFQRQQEAKELRQQYQDYYRAFQAKRKGKK KPKVLILMGLPGSYLVATNQSYVGNLLDLAGGENVYQSDEKEFLSAN PEDMLAKEPDLILRTAHAIPDKVKVMFDKEFAENDIWKHFTAVKEGK VYDLDNTLFGMSAKLNYPEALDTLTQLFDHVGD**A**P]]	35363.9
MGGSHHHHHHGMASMTGGQQMGRDLYDDDDK[DR[WGSELEVNQ HPKTAKETEQQRIVATSVAVVDICDRLNLDLVGVCDSKLYTLPKRYD AVKRVGLPMNPDIELIASLKPTWILSPNSLQEDLEPKYQKLDTEYGFL NLRSVEGMYQSIDDLGNLFQRQQEAKELRQQYQDYYRAFQAKRKGK KKPKVLILMGLPGSYLVATNQSYVGNLLDLAGGENVYQSDEKEFLSA NPEDMLAKEPDLILRTAHAIPDKVKVMFDKEFAENDIWKHFTAVKEG KVYDLDNTLFGMSAKLNYPEALDTLTQLFDHVGD**A**_]]	35455.0
GGSHHHHHHGMASMTGGQQMGRDLYDDDDK[DR[WGSELEVNQH PKTAKETEQQRIVATSVAVVDICDRLNLDLVGVCDSKLYTLPKRYDA VKRVGLPMNPDIELIASLKPTWILSPNSLQEDLEPKYQKLDTEYGFLN LRSVEGMYQSIDDLGNLFQRQQEAKELRQQYQDYYRAFQAKRKGKK KPKVLILMGLPGSYLVATNQSYVGNLLDLAGGENVYQSDEKEFLSAN PEDMLAKEPDLILRTAHAIPDKVKVMFDKEFAENDIWKHFTAVKEGK VYDLDNTLFGMSAKLNYPEALDTLTQLFDHVGD**A**]]	35323.8

Figure 26. The molecular weight of mutant SiaA, H229A – Met, H229A – (Met + Gly), H229A – Pro, and H229A – (Met + Pro).

	SiaA (Da)	SiaA - Met (Da)	SiaA - (Met + Gly) (Da)	SiaA – Pro (Da)	SiaA - (Met + Pro) (Da)
WT SiaA	35618	35487	35430	35521	35390
H229A	35552	35421	35364	35455	35324
F33 (Da)	35441 ± 0.056 %		**MALDI error (0.05%) (Da)**	± 17	
Na + (Da)	22		**ESI error (0.02%) (Da)**	± 7	

Figure 27. The expected molecular weight (MW) of H229A is 35552.3 Da. The actual MW of mutant SiaA (H229A – Met) is 35421 Da. The MW of fraction 33, H229A, is 35441 Da. It is heavier than the H229A – Met by 20 Da, which is close to the MW of a sodium ion.

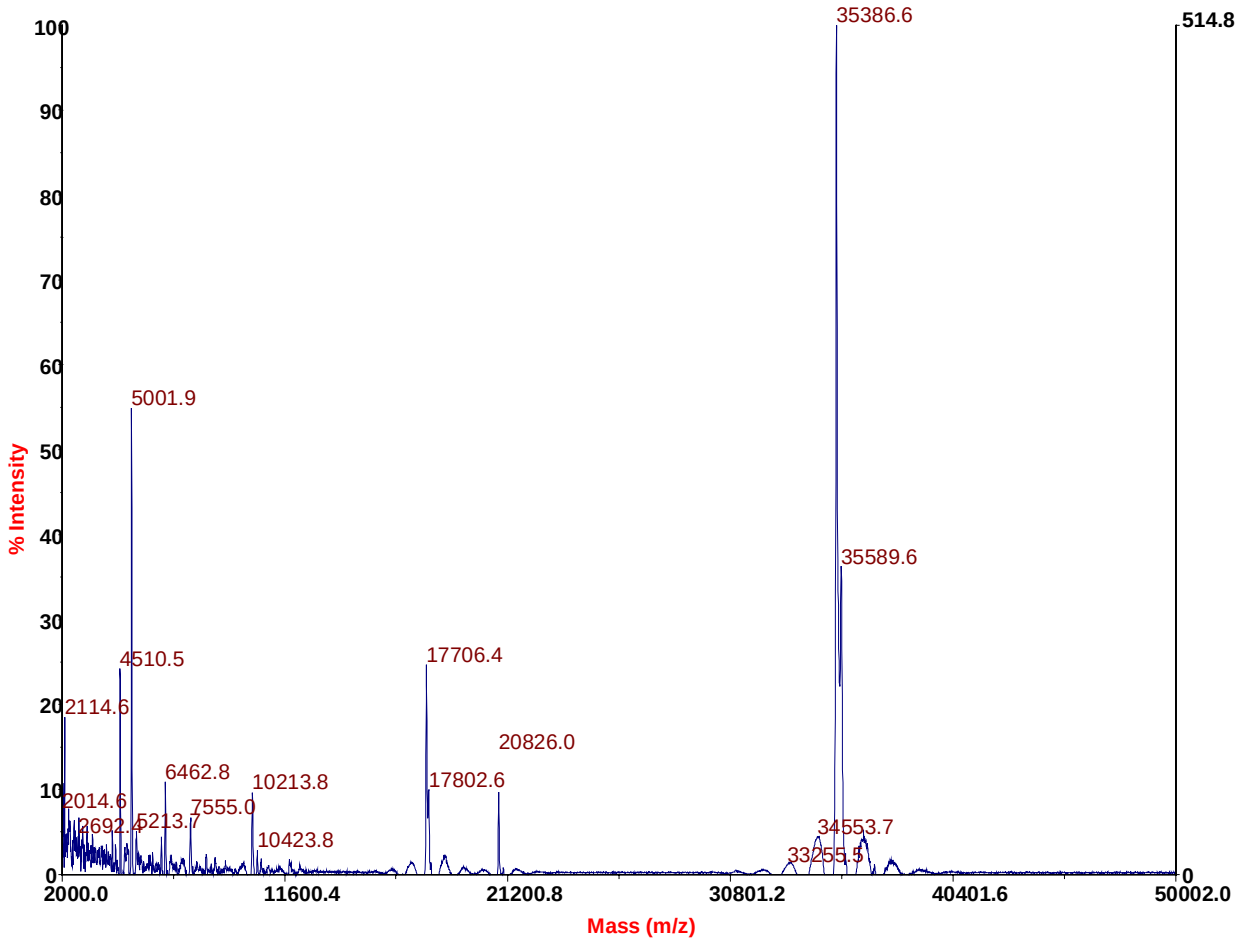

Figure 28. MALDI mass spectrometry of fraction 32 after desalting. The tallest peaks are at 35386.6 Da and 35589.6 Da. Both molecular weights are heavier than that observed in the saltier sample (Figure 22). The theoretical weight of H229A SiaA is 35552.2.

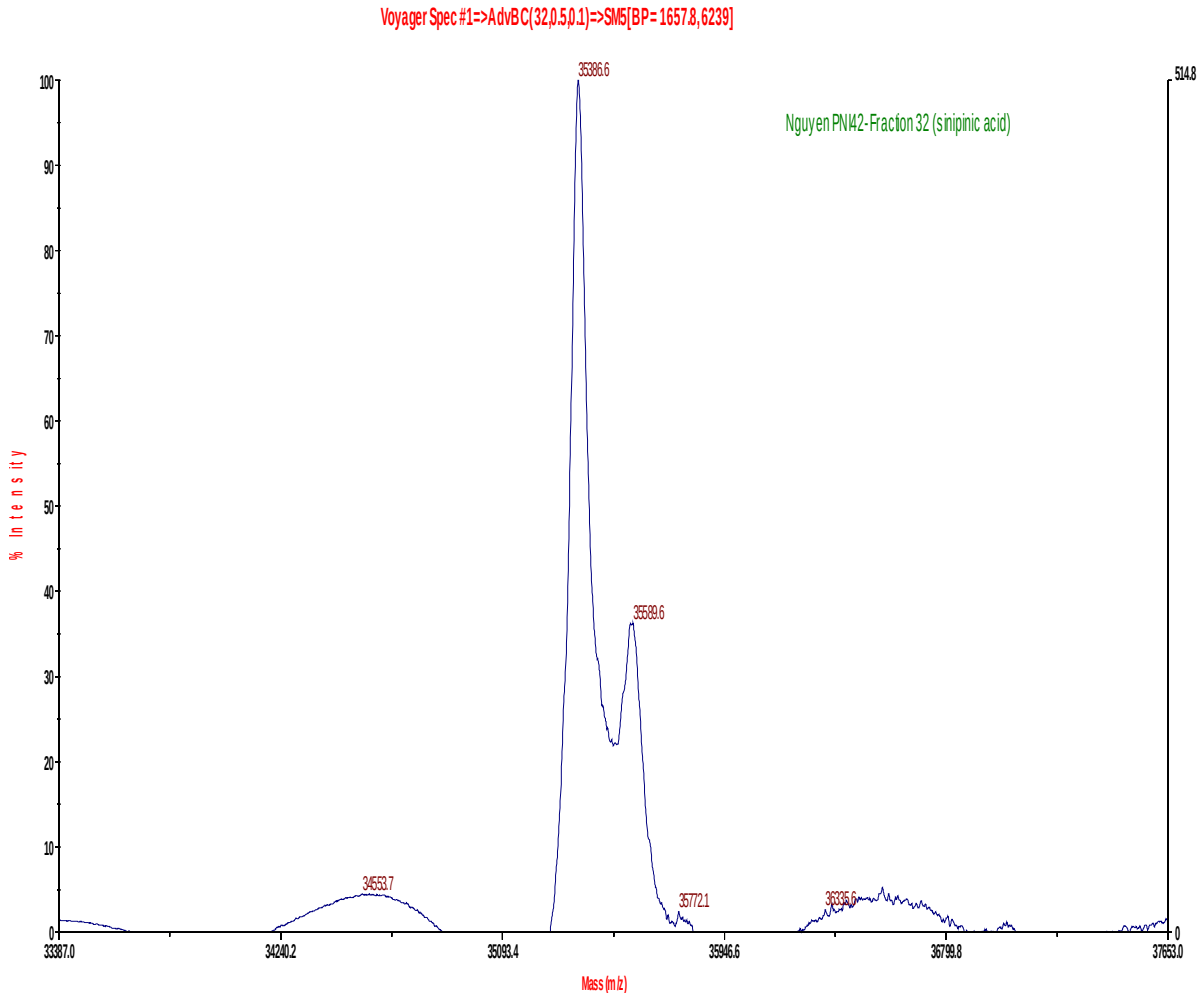

Figure 29. Close-up of the major peak from Figure 24.

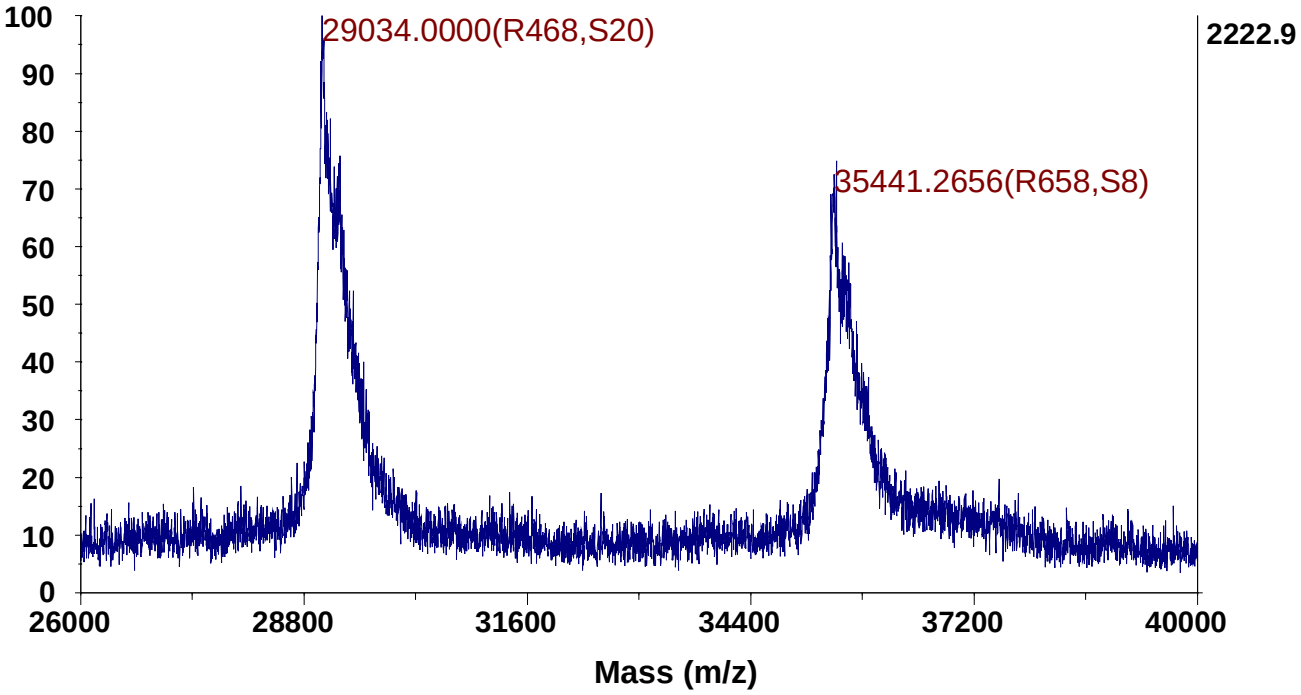

Figure 30. MALDI mass spectrum of fraction 33 from Figure 21. The tallest peak is at 35441 Da. Carbonic anhydrase was used for internal standard.

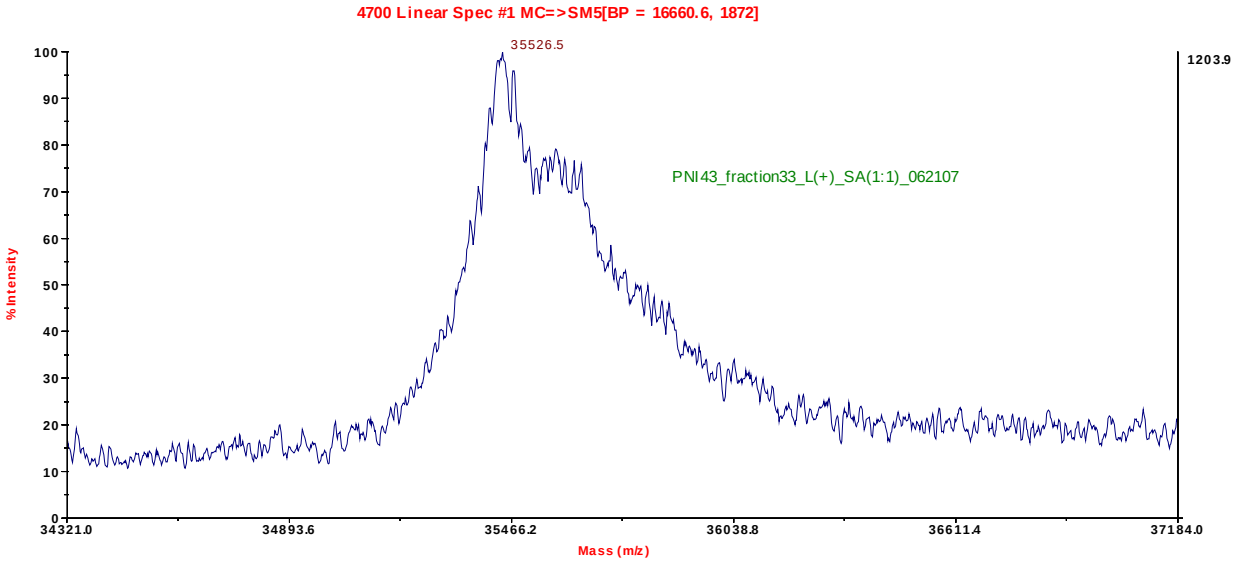

Figure 31. MALDI mass spectrometry of fraction 33 after desalting. The tallest peak is at 35526.5 Da. The molecular weight is heavier than the salting sample.

	Abs	**Abs**				
Fraction	**280 nm**	**409 nm**	**Experimental ratio**	**Fraction holo**	**[Holo]**	**grams**
27	0.55	0.12	0.22	0.13	1.2E-06	8.5E-05
28	0.55	0.12	0.22	0.13	1.2E-06	8.5E-05
29	0.65	0.16	0.25	0.15	1.6E-06	1.1E-04
30	0.85	0.25	0.29	0.18	2.5E-06	1.8E-04
31	0.89	0.27	0.30	0.18	2.7E-06	1.9E-04
32	0.73	0.20	0.27	0.16	2.0E-06	1.4E-04
33	0.57	0.12	0.21	0.13	1.2E-06	8.5E-05
		Avg	0.25	0.15		8.8E-04
		SD	0.039			
Assumes that each fraction is 2.0 mL,						
that the extinction coefficient at the Soret is 1 x 10^5 M^{-1} cm^{-1}						
and the 409/280 nm ratio for holoprotein is 1.67						
The expected molecular weight of the protein is 35,552.						
Total protein 5.9 mg						

Figure 32. Absorbances at 280 and 409 nm for fractions 27 - 33, allowing calculation of the fraction of holoprotein, the molarity of holoprotein, and the weight of holoprotein for each fraction. Totals are also given.

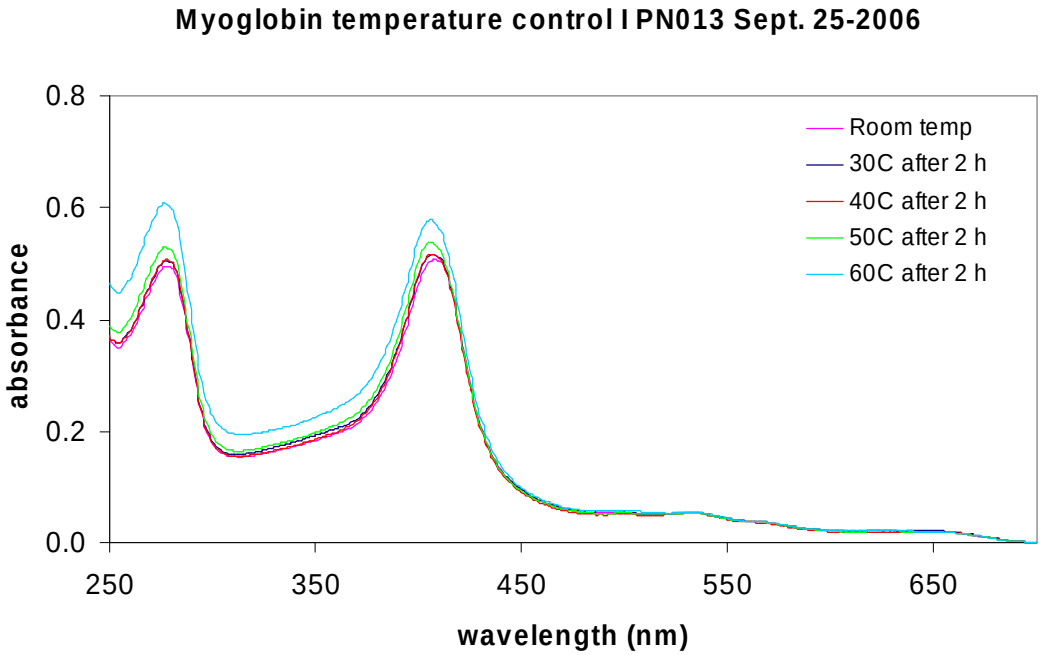

Figure 33. Horse heart myoglobin in phosphate buffer as a function of temperature. The temperature was held at each point for 2 h. The temperature was increased during the run. The Soret band increases as the temperature increases up to 60 °C in this experiment.

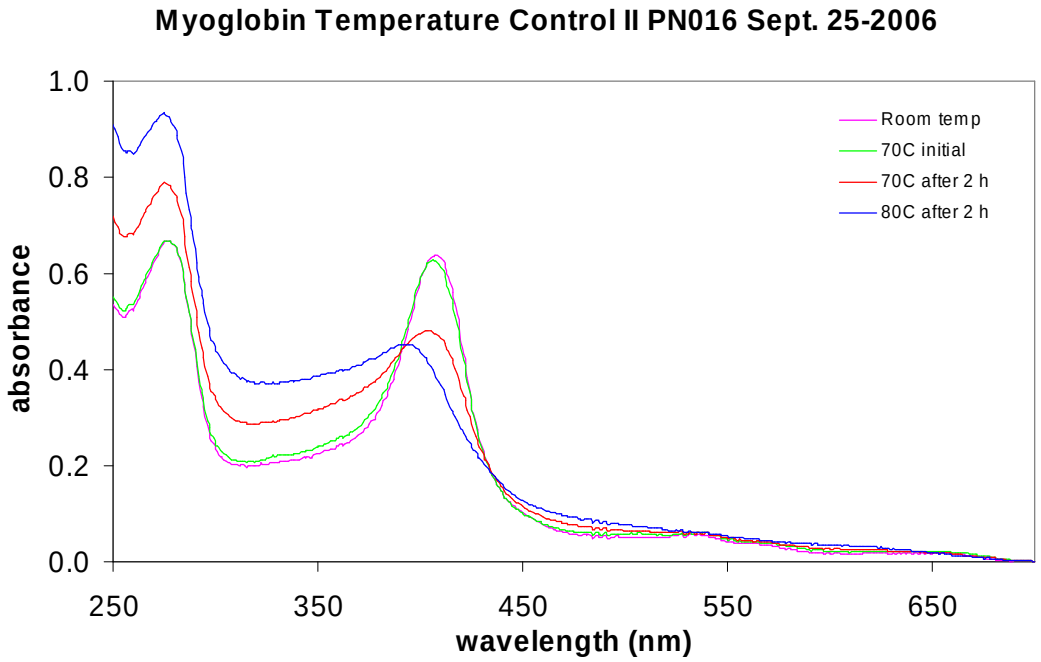

Figure 34. Horse heart myoglobin in phosphate buffer as a function of temperature. The temperature was held at each point for 2 h. The temperature was increased during the run. When the sample was kept at 70 °C for 2 h, the Soret band decreased in intensity. A further decrease was seen on heating to 80 °C.

$$y_{obs} = \frac{(y_n + m_n T) + (y_d + m_d T)\{\exp[\Delta H_m / R \cdot (1/T_m - 1/T)]\}}{\{1 + \exp[\Delta H_m / R \cdot (1/T_m - 1/T)]\}}$$

$$\mathbf{y_{obs} = \frac{(m1+m2*m0)+(m3+m4*m0)*(exp((m5/1.987)*((1/m6)-(1/m0))))}{(1+exp((m5/1.987)*((1/m6)-(1/m0))))}}$$

Figure 35. (Top) Thermal denaturation equation (Swint & Robertson, 1993). (Bottom) Thermal denature equation defined in Kaleidagraph. The experimental absorbance is y_{obs}. T (m0) is the temperature in Celsius; R is the gas constant (R = 1.987 (J/(mol*K)); ΔH_m (m5) is the enthalpy; and T_m (m6) is the melting temperature. The y-intercepts of the folded and unfolded baselines are y_n (m1) and y_d (m3), respectively. The slopes of the baselines are m_n (m2) and m_d (m4), respectively.

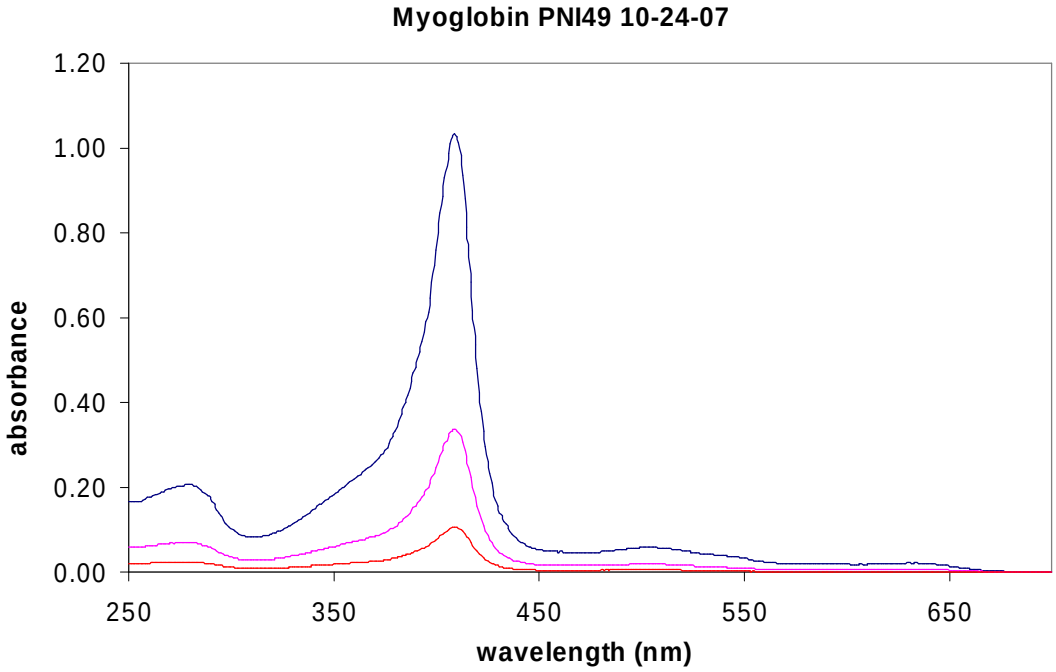

Figure 36. Equine skeletal muscle myoglobin in phosphate buffer. At OD_{409}, the absorbance for the original sample, 1:3 dilution, and 1:0 dilution are 1.04, 0.34, and 0.11, respectively.

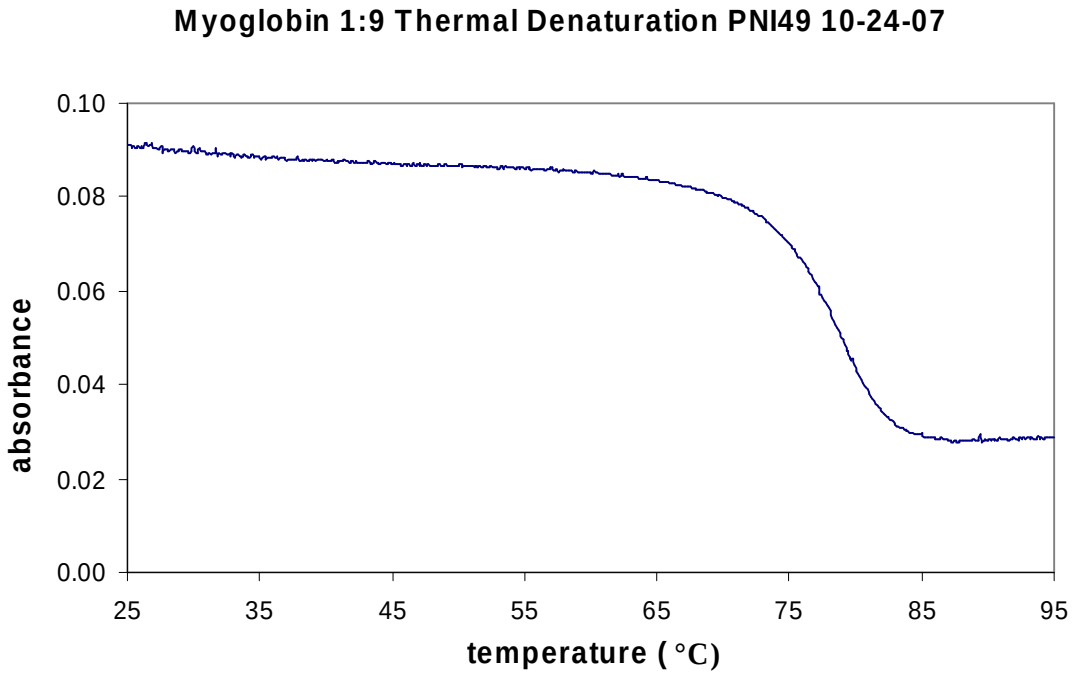

Figure 37. The absorbance at 409 nm of equine skeletal muscle myoglobin in 50 mM, pH 7.1 phosphate buffer as a function of temperature.

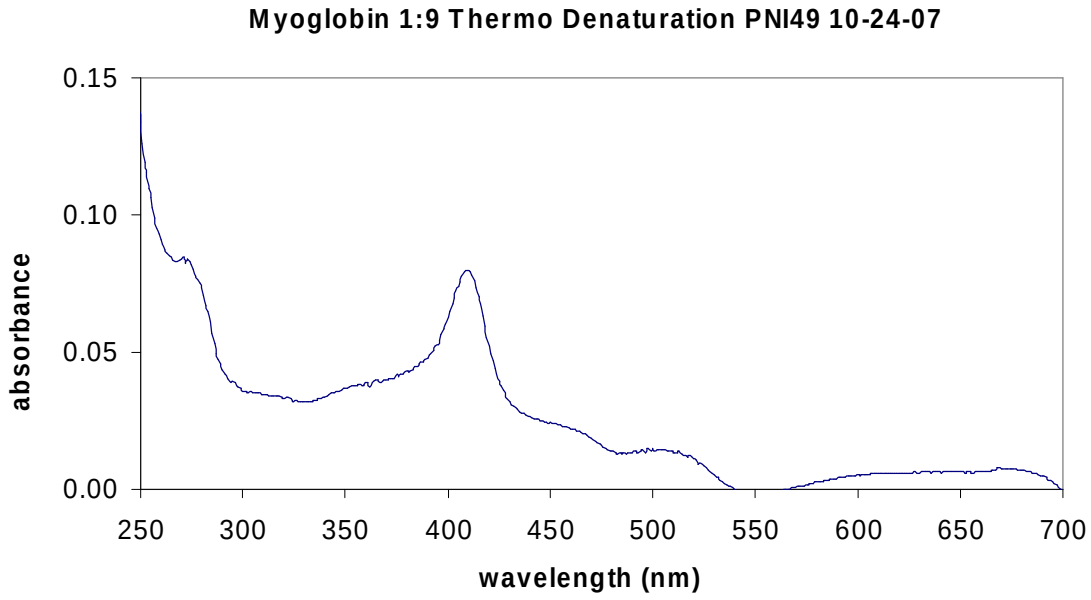

Figure 38. The absorbance of equine skeletal muscle myoglobin in 50 mM phosphate buffer, pH 7.1 at room temperature after thermal denaturation.

Trial	m1 (native) (abs)	m2 (folding slope) (abs/°C)	m3 (unfolding) (abs)	m4 (unfolding slope) (abs/°C)	m5 (ΔH) (J)	m6 (melting temp) (°C)
1	0.9	-0.0001518	0.02125	0.0001086	10000	78
2	0.91	-0.0001518	0.02125	0.0001086	8000	78
3	0.91	-0.0001618	0.022	0.0001086	8000	78.5
4	0.91	-0.0001718	0.0225	0.0001086	7000	78.5
5	0.91	-0.0001818	0.03	0.0001086	7000	78.8
6	0.91	-0.0001818	0.015	0.0001086	4600	78.8
7	0.95	-0.00018	0.01	0.0001086	4600	78.8
8	0.95	-0.00018	0.005	0.0001086	4600	78.8
9	0.95	-0.00018	0.0001	0.0001086	4600	78.8
10	0.95	-0.00018	0	0.0001086	4600	78.8

Trials	m1 (native) (abs)	m2 (folding slope) (abs/°C)	m3 (unfolding) (abs)	m4 (unfolding slope) (abs/°C)	m5 (ΔH) (J)	m6 (melting temp) (°C)	R
1	0.108 ±5.466e-4	-0.000420 ±1.067e-5	0.0238 ±7.428e-3	0.0000510 ±8.339e-5	9735 ±557	78.3 ±0.05	0.99052
2	0.0951 ±1.169e-4	-0.000177 ±2.401e-6	-0.0320 ±3.056e-3	0.000648 ±3.311e-5	4611 ±41	78.8 ±0.05	0.99964
3	0.0951 ±1.169e-4	-0.000177 ±2.401e-6	-0.0320 ±3.053e-3	0.000648 ±3.311e-5	4611 ±41	78.8 ±0.05	0.99964
4	0.0951 ±1.169e-4	-0.000177 ±2.401e-6	-0.0320 ±3.053e-3	0.000648 ±3.311e-5	4611 ±41	78.8 ±0.05	0.99964
5	0.0951 ±1.169e-4	-0.000177 ±2.401e-6	-0.0322 ±3.055e-3	0.000650 ±3.311e-5	4609 ±41	78.8 ±0.05	0.99964
6	0.0951 ±1.169e-4	-0.000177 ±2.401e-6	-0.0322 ±3.055e-3	0.000650 ±3.314e-5	4609 ±41	78.8 ±0.05	0.99964
7	0.0951 ±1.169e-4	-0.000177 ±2.401e-6	-0.0320 ±3.053e-3	0.000648 ±3.311e-5	4611 ±41	78.8 ±0.05	0.99964
8	0.0951 ±1.169e-4	-0.000177 ±2.401e-6	-0.0320 ±3.053e-3	0.000648 ±3.311e-5	4611 ±41	78.8 ±0.05	0.99964
9	0.0951 ±1.169e-4	-0.000177 ±2.401e-6	-0.0320 ±3.053e-3	0.000648 ±3.311e-5	4611 ±41	78.8 ±0.05	0.99964
10	0.0951 ±1.169e-4	-0.000177 ±2.401e-6	-0.0320 ±3.053e-3	0.000648 ±3.311e-5	4611 ±41	78.8 ±0.05	0.99964
AVG	0.0951 ±1.169e-4	-0.000177 ±2.401e-6	-0.0321 ±3.053e-3	0.000649 ±3.312e-5	4611 ±41	79 ±0.1	0.99964

Figure 39. Kaleidagraph data fitting. (Top) For each trial, the value for each variable was estimated and put into thermal denaturation equation (Figure 37). The fitted values are shown in the lower half of the table.

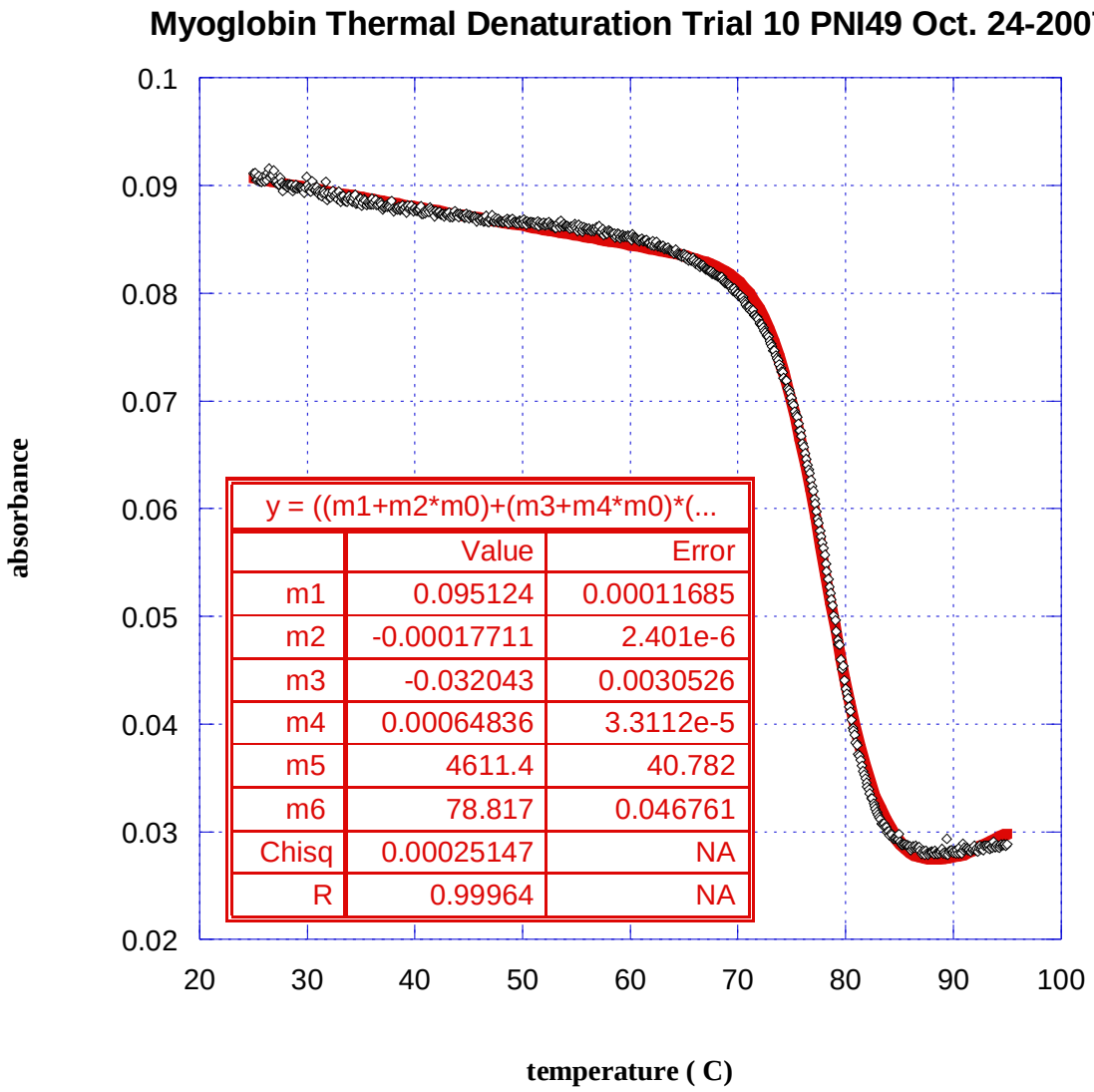

Figure 40. Kaleidagraph curve fit for Trial 10.